

**VESKLER AND BALDIN LABORATORY OF HIGH ENERGY PHYSICS
JOINT INSTITUTE OF NUCLEAR RESEARCH
DUBNA, RUSSIA**

**Study of Pion Interferometry in Au-Au collision in STAR
Experiment at $\sqrt{s_{NN}} = 7.7$ GeV**

**FINAL PROJECT REPORT
START PROGRAM**

Submitted By:

Nishant Gaurav

Indian Institute of Science Education and Research Kolkata

Submitted To:

Mr. Vinh Loung

Veskler and Baldin Laboratory of High Energy Physics

Joint Institute of Nuclear Research

Dubna, Russia

July 02 - August 12, 2023

ABSTRACT

Pion Femtoscopy, a sophisticated technique in particle physics, is employed to unveil correlations among pion particles from the source's homogeneity region. Our analysis of collider data from the STAR BES II experiment, focusing on $\sqrt{s_{NN}} = 7.7$ GeV collisions, explores the correlation function across centrality and transverse momentum (K_T) intervals. To ensure robust results, I meticulously manage track effects using tailored cuts derived from the splitting level and fraction of merged rows. My investigation extends to understanding the correlation function's behavior with varying numbers of Vz bins during event mixing and its response to different Vz ranges for analysis. Integral to my study is the fitting of the Bowler-Sinyukov function to the correlation function. This yields essential parameters: radii characterizing the source's homogeneity region and correlation strength for positive and negative pions. These parameters offer insights into the particle-emitting environment's dimensions and inter-pion correlations. Additionally, I explore parameter variation in response to changing centrality conditions, deepening my understanding of collision characteristics' impact on the source's behavior.

ACKNOWLEDGEMENT

This project is prepared in fulfilment of the requirement for the START program at JINR. I owe my deepest gratitude to the STAR group at Veskler and Baldin Laboratory of High Energy Physics, Joint Institute of Nuclear Research for providing me with an opportunity through the START program to work on this project.

I also extend my gratitude towards my project supervisor and mentor, Mr Vinh Loung whose guidance and expertise have been invaluable in steering me towards success. Any amount of thank would be insufficient for his continuous support and encouragement that has made it possible for me to progress significantly and dig deeply in the topic even in this short time span. I also thank Dr Alexey Aparin and Dr Ivonne Alicia Maldonado Cervantes for their valuable feedback and suggestions.

Finally, I would like to thank my friends Santiago Bernal Langarica, Rodrigo García Formentí Mendieta, Rodrigo Guzmán Castro, José Jorge Medina Serna for their constant encouragement throughout the START program. I acknowledge the contributions of everyone who supported me in the creation of this project report.

Thank you all for your assistance and support.

The experience of working on this project has not only enriched my technical knowledge and analytical skills, and also give me hands on experience of working on the physics of pion femtoscopy and help develop my team's skill set to a great extent.

TABLE OF CONTENTS

ABSTRACT	i
ACKNOWLEDGEMENT	ii
1 INTRODUCTION	1
1.1 STAR Experiment	1
1.2 STAR Detector	2
1.2.1 Time Projection Chamber (TPC)	3
1.2.2 Time-of-Flight (TOF) Detector	3
1.2.3 Barrel Electro-Magnetic Calorimeter (BEMC) and Endcap Electro-Magnetic Calorimeter (EMC)	3
1.3 Experimental Techniques	3
1.3.1 Particle Ratios and Abundance	4
1.3.2 Anisotropic Flow	4
1.3.3 Hanbury Brown-Twiss (HBT) Correlations: Pion Femtoscopy	4
1.3.4 Jet Quenching and Parton Energy Loss	4
2 PION FEMTOSCOPY	5
2.1 Why Pions?	5
2.1.1 Principles of Pion Femtoscopy	6
2.1.2 The Hanbury Brown-Twiss Effect	6
2.1.3 Interferometry and Spatial Correlations	6
2.1.4 Correlation Function and Femtoscopy	6
2.2 Pion Source Function and Source Size	7
2.3 Interferometry and Extraction of Radii	7
3 METHODOLOGY	8
3.1 Event Selection	8
3.2 Pion Identification	8
3.3 Relative Momentum Analysis	9
4 CORRELATION FUNCTION	10
4.1 Centrality and K_T Dependence of Correlation Function	10
4.2 Dependence of CF on number of Vz bins	13
5 TRACK EFFECTS	16
5.1 Splitting Level	16
5.2 Fraction of Merged Rows	19

6 ANALYSIS OF CORRELATION FUNCTION	22
6.1 Dependence of Correlation Function on Vz range	22
6.2 Fitting of Correlation Function	27
7 CONCLUSION	30
References	33
A APPENDIX	34
A.1 Event Selection	34
A.2 Track Selection	35
A.3 Particle Identification	36
A.4 Centrality	38

1. INTRODUCTION

In the grand quest to comprehend the fundamental building blocks of the universe, one of the most enigmatic and elusive states of matter that has captured the attention of physicists is Quark-Gluon Plasma (QGP). This remarkable form of matter is believed to have existed in the immediate aftermath of the Big Bang, providing a glimpse into the earliest moments of our universe's evolution. At the forefront of the scientific endeavor to explore QGP lies the Solenoidal Tracker at RHIC (STAR) experiment, a colossal collaborative effort conducted at the Relativistic Heavy Ion Collider (RHIC) at Brookhaven National Laboratory in New York. To comprehend the significance of QGP and its relation to the STAR experiment, one must delve into the nature of matter at its most fundamental level. At the heart of all visible matter, such as protons and neutrons, lie elementary particles called quarks, held together by the strong nuclear force mediated by gluons. These quarks and gluons are the constituents of hadrons, the particles that make up the building blocks of everyday matter.

Under normal circumstances, these quarks and gluons are confined within hadrons due to the forceful nature of the strong force. However, during the universe's infancy, in the astonishingly high-energy environment that prevailed moments after the Big Bang, the temperature and energy density were so extreme that quarks and gluons roamed freely, unbound by the confines of hadrons. This extraordinary state of matter, akin to a primordial "soup" of quarks and gluons, is known as Quark-Gluon Plasma. QGP is believed to have been present during the universe's first microseconds and persisted until the universe expanded and cooled sufficiently to form hadrons. The fleeting existence of this primordial state renders it exceptionally difficult to study directly. Nonetheless, scientists are determined to recreate QGP under laboratory conditions, shedding light on the early universe and deepening our understanding of the fundamental forces that govern the cosmos.

1.1. STAR Experiment

The Solenoidal Tracker at RHIC (STAR) is a state-of-the-art experiment designed to explore the properties of Quark-Gluon Plasma (QGP) and gain insights into the early moments of the universe's evolution. Located at the Relativistic Heavy Ion Collider (RHIC) at Brookhaven National Laboratory in New York. The STAR experiment, a flagship undertaking within the field of nuclear physics, seeks to recreate and study the properties of QGP by colliding heavy ions at ultra-high energies. RHIC, the platform on which the STAR experiment is conducted, is a marvel of scientific engineering, capable of accelerating and colliding heavy nuclei, such

as gold or copper, at velocities close to the speed of light. By subjecting these heavy ions to high-energy collisions, the STAR experiment endeavors to replicate the extreme conditions of the early universe, albeit on a vastly smaller scale. The collisions generate a minuscule fireball of energy, liberating the constituent quarks and gluons from the nuclei, and momentarily recreating the fleeting state of Quark-Gluon Plasma. As the fireball rapidly expands and cools, the liberated quarks and gluons combine to form hadrons, which can be measured and analyzed by the experiment's detectors. The creation and study of QGP is particularly challenging since it exists for only a fraction of a second before transitioning into hadrons, the particles that constitute everyday matter. The STAR experiment aims to detect and analyze the particles emitted during these heavy-ion collisions to obtain valuable information about the properties and characteristics of the QGP fireball.

1.2. STAR Detector

The STAR detector is a complex and multi-layered instrument, specifically designed to capture and measure the properties of particles produced in heavy-ion collisions. The detector is situated at the intersection point of the colliding ions, allowing it to capture the emergent particles effectively. The STAR detector is composed of several sub-detectors, each with its specialized function to record the myriad particles generated during the collision events.

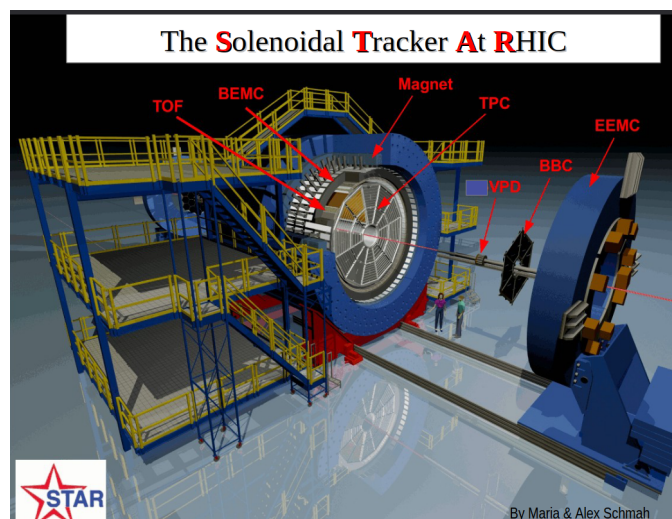


Figure 1.1: Schematic diagram of STAR detector (by Maria & Alex Schmah)

1.2.1. Time Projection Chamber (TPC)

At the core of the STAR detector lies the Time Projection Chamber (TPC), one of the most vital components of the experiment. The TPC is an enormous cylindrical device filled with a gas mixture, surrounded by a strong magnetic field produced by a solenoid magnet. When charged particles pass through the gas volume, they ionize the gas, releasing electrons. These electrons drift towards endplates, which are equipped with sensitive electronic readout chambers. By tracking the path and curvature of these drifting electrons, the TPC reconstructs the trajectory and momentum of the charged particles produced in the collision. This capability allows scientists to identify and measure the properties of various particles, including pions, protons, and other hadrons, which carry crucial information about the QGP medium.

1.2.2. Time-of-Flight (TOF) Detector

Complementing the TPC is the Time-of-Flight (TOF) detector, an essential sub-detector that measures the time taken by charged particles to travel from the interaction point to the TOF detectors. By combining this time-of-flight information with the momentum and charge of the particles measured by the TPC, scientists can calculate the particle's velocity. Accurate velocity measurements aid in particle identification, helping to distinguish between different particle species.

1.2.3. Barrel Electro-Magnetic Calorimeter (BEMC) and Endcap Electro-Magnetic Calorimeter (EEMC)

In addition to the EMC, the STAR detector is equipped with the Barrel Electromagnetic Calorimeter (BEMC) and the Endcap Electromagnetic Calorimeter (EEMC). These calorimeters extend the EMC's coverage, providing a more comprehensive measurement of electromagnetic particles and interactions.

1.3. Experimental Techniques

The complex and highly sophisticated nature of the STAR detector enables the implementation of advanced experimental techniques to study the QGP medium and its characteristics.

1.3.1. Particle Ratios and Abundance

One of the fundamental experimental techniques used in heavy-ion experiments is the measurement of particle ratios and abundance. The relative abundance of various particles, such as pions, kaons, and protons, provides valuable information about the conditions and composition of the QGP fireball. Deviations from expected ratios can hint at novel phenomena occurring during the QGP phase.

1.3.2. Anisotropic Flow

Another crucial observable is anisotropic flow, which refers to the preferential emission of particles in certain directions relative to the collision's symmetry axis. This phenomenon arises due to the collective motion of the QGP medium, which can be characterized by different harmonic orders. The study of anisotropic flow patterns allows scientists to gain insights into the QGP's transport properties and the interactions among its constituents.

1.3.3. Hanbury Brown-Twiss (HBT) Correlations: Pion Femtoscopy

Pion femtoscopy, based on Hanbury Brown-Twiss (HBT) correlations, is a powerful experimental technique used in heavy-ion experiments, particularly in the study of QGP. By analyzing the angular correlations and relative momenta of pion pairs emitted from the collision, scientists can deduce information about the size, shape, and lifetime of the QGP fireball. This technique provides crucial insight into the collective behavior of the QGP medium and the expansion dynamics of the fireball. The exploration of this technique is also the main goal of our project.

1.3.4. Jet Quenching and Parton Energy Loss

Another intriguing phenomenon explored in heavy-ion collisions is jet quenching, which refers to the energy loss experienced by high-energy partons (quarks or gluons) as they traverse the QGP medium. The STAR experiment and its advanced detectors enable the study of jet quenching, shedding light on the properties of the QGP and its interactions with the produced partons.

2. PION FEMTOSCOPY

Pion femtoscopy is a powerful and sophisticated experimental technique used in heavy-ion collision experiments to study the spatial and temporal characteristics of Quark-Gluon Plasma (QGP). As one of the most abundant and readily detected particles produced during these high-energy collisions, pions carry essential information about the medium's expansion dynamics and interactions. By analyzing the correlations between pion pairs, researchers gain valuable insights into the size, shape, and lifetime of the QGP fireball. This detailed overview will delve into the intricacies of pion femtoscopy, its underlying principles, and its significance in unraveling the mysteries of QGP. During this brief moment of time, the universe was filled with a hot, dense "soup" of quarks and gluons, known as QGP. As the universe rapidly expanded and cooled, the quarks and gluons combined to form protons, neutrons, and other hadrons, which constitute the matter we observe today. The fleeting existence of QGP makes it exceptionally challenging to study directly. However, through the recreation of QGP conditions in heavy-ion collisions, experiments like the Solenoidal Tracker at RHIC (STAR) aim to provide valuable insights into the properties of this elusive state of matter.

2.1. Why Pions?

Pions are mesons composed of a quark and an antiquark. As the lightest hadrons, pions are produced abundantly in heavy-ion collisions, making them essential probes for studying the properties of the medium created during the QGP phase. Due to their relatively long lifetimes compared to other particles produced in the collisions, pions can traverse the expanding QGP fireball and its subsequent hadronic stage without undergoing significant interactions. Thus, they carry crucial information about the medium's size, shape, and duration.

Pions can be categorized into two main types based on their charge: positively charged (π^+) and negatively charged (π^-). Additionally, there are neutral pions (π^0) that decay almost instantly into two photons. The measurement of pion properties, such as their momenta, trajectories, and emission angles, is crucial for conducting pion femtoscopy and extracting information about the QGP medium.

2.1.1. Principles of Pion Femtoscopy

2.1.2. The Hanbury Brown-Twiss Effect

The foundation of pion femtoscopy lies in the Hanbury Brown-Twiss (HBT) effect, which was initially developed in the context of astronomy and later adapted for the study of particles in nuclear and high-energy physics. The HBT effect is a phenomenon related to the quantum statistics of identical particles, such as pions, that are emitted from the same collision source.

In the case of heavy-ion collisions, the source of emitted particles is the QGP medium, which expands and evolves rapidly. Due to quantum statistics, identical pions tend to exhibit a higher probability of being emitted in close proximity to each other, with similar momenta and directions. Conversely, pairs of pions that are non-identical do not exhibit this quantum statistical correlation.

2.1.3. Interferometry and Spatial Correlations

To understand the spatial correlations of emitted pions, interferometry concepts are employed. Imagine two detectors placed at different positions relative to the collision source. If two pions are emitted from the same location in the QGP medium, they have a higher probability of being detected by the same detector (coincidence). Conversely, if the pions come from different sources, they are less likely to be detected together.

The correlation function, denoted as $C(q)$, quantifies this probability of detecting two pions with a relative momentum q . The relative momentum of the two pions is denoted by $q = p_1 - p_2$, where p_1 and p_2 are the momenta of the individual pions. The correlation function is inversely related to the spatial distribution of the particle source. By analyzing the $C(q)$ function, researchers can extract information about the spatial size and shape of the source, effectively providing a snapshot of the QGP medium at the moment of particle emission.

2.1.4. Correlation Function and Femtoscopy

The fundamental principle behind pion femtoscopy lies in the study of the two-particle correlation function, which quantifies the probability of detecting two pions as a function of their relative momentum. This correlation function provides insight into the spatial and temporal evolution of the QGP medium during its expansion phase.

The correlation function is defined as the ratio of probability of observing two particles together to the product of probabilities of observing two particles separately. Mathematically, it is given by:

$$C(q) = \frac{P(p_1, p_2)}{P(p_1)P(p_2)},$$

where $C(q)$ is the correlation function, $P(p_1, p_2)$ is the probability of observing two-particle together, and $P(p_1)$ and $P(p_2)$ are the probabilities of observing the particle 1 and particle 2 separately.

2.2. Pion Source Function and Source Size

The pion source function, $S(r)$, describes the probability of emitting two pions from a given position, r , in the QGP medium. The HBT correlation function is related to the pion source function through a Fourier transformation. By analyzing the shape of the correlation function, one can extract information about the size and shape of the pion-emitting source.

The source size parameters can be quantified in terms of the HBT radii, which describe the spatial extensions of the source along three orthogonal axes: the outward (R_{out}), sideward (R_{side}), and longitudinal (R_{long}) directions. The R_{out} and R_{side} radii correspond to the size of the fireball at the time of pion emission, while the R_{long} radius characterizes the time duration of the particle emission process.

2.3. Interferometry and Extraction of Radii

The analysis of pion femtoscopy involves performing an interferometric measurement on the emitted pion pairs. The interference between identical particles results in the modulation of the correlation function at low relative momenta, creating a characteristic oscillatory pattern. The radius parameters can be extracted by fitting the correlation function with a suitable functional form, such as a Gaussian or an exponential fit.

Several methods are used to extract the radii from the correlation function, including the Bertsch-Pratt method and the Yano-Koonin-Podgoretskii (YKP) method. These techniques provide complementary information and help validate the results obtained using different approaches. In this report, the correlation function is fitted using Bowler-Sinyukov function for extract the information about radius and correlation strength.

3. METHODOLOGY

3.1. Event Selection

Pion femtoscopy relies on collecting large datasets of heavy-ion collision events. The STAR experiment at RHIC is ideally suited for this purpose, as it can generate a substantial number of events with heavy ions such as gold or copper nuclei colliding at ultra-high energies. The selection of relevant events for pion femtoscopy analysis is crucial to ensure that only events with particle emissions from the QGP medium are considered. The data used for the current analysis is from Au-Au collision experiment at $\sqrt{s_{NN}} = 7.7$ GeV and with approximately 1.9M events.

1. Event Selection:

- Radial Collision Vertex Cut, $V_r < 2$ cm
- z-position of collision vertex cut, $|V_z| < 145$ cm

2. Track Selection:

- Number of TPC hits used for track reconstruction: $N_{hits}^{fits} \geq 15$
- Consider only primary track
- Distance of closest approach (DCA), $|DCA| < 3$ cm
- Total momentum of the primary track, $0.15 < p_{tot}^{prim} < 1.5$ GeV/c
- Transverse momentum of the primary track, $0.15 < p_T^{prim} < 1.5$ GeV/c
- Pseudorapidity of the primary track, $|\eta| < 1.5$

3.2. Pion Identification

Identifying pions among the multitude of particles produced in heavy-ion collisions is a critical step in pion femtoscopy. Particle identification is achieved using detectors like the Time Projection Chamber (TPC) and the Time-of-Flight (TOF) detector. The TPC measures the ionization of particles passing through the gas volume, providing information on their momenta, while the TOF detector measures the time taken by particles to travel to specific detectors. By combining the information from both detectors, researchers can accurately identify pions and separate them from other particle species.

1. For $0.15 < p_{tot}^{prim} < 0.55$ GeV/c (TPC-only identification)
 - $|n\sigma(\pi)| < 2$
 - $|n\sigma(e)| > 2$
 - $|n\sigma(K)| > 2$
 - $|n\sigma(p)| > 2$
2. For $0.55 < p_{tot}^{prim} < 1.5$ GeV/c (TPC+TOF identification)
 - $|n\sigma(\pi)| < 3$
 - $1/\beta - 1/\beta_{\pi}^{expected} < 0.015$
 - $-0.05 < m^2 < 0.08 GeV^2/c^4$

3.3. Relative Momentum Analysis

To study the correlations between pion pairs, we examine the relative momentum of the pions in the laboratory frame. This involves determining the momenta of the two pions in the pair and then calculating their relative momentum vector, $q = p_1 - p_2$, where p_1 and p_2 are the momenta of the individual pions. The correlation function $C(q)$ is then constructed by comparing the number of observed pion pairs with a given relative momentum q to the number of pairs expected for uncorrelated pions.

Experimentally, the correlation function (CF) is defined as

$$CF = \frac{Signal}{Background},$$

where signal implies the values of q for pair of particles coming from same events while background constitutes of q for pair of particles coming from different events. Among the several methods of creating the background, the event mixing method is used in this report. The q for background is chosen from the pair of pions which belong to similar V_z and multiplicity distribution. This helps in considering the most relevant particles pairs to be chosen as background while maintaining the good statistics at the same time.

The multiplicity has been divided into 30 bins for event mixing where each region consists of multiplicity of order 10. Whereas for the V_z (-145 to 145 cm) case, it is divided into 58 bins with each bin width is 5 cm. The correlation function is constructed by dividing the signal with background with suitable normalization as the background will have higher number of entries than the signal.

4. CORRELATION FUNCTION

The interesting cases for studying is correlation functions comes from choosing some particular conditions to infer the information of source sizes. The CF is studied by choosing the event centralities into the following categories:

- 0 - 10%
- 10 - 30%
- 30 - 50%
- 50 - 80%

Another interesting quantity is K_T which is defined as

$$K_T = \left| \frac{p_T^1 + p_T^2}{2} \right|,$$

where p_T^1 and p_T^2 are the transverse momenta of individual pions. The interesting cases for K_T dependence are

- $0.15 \leq K_T < 0.25$ GeV/c
- $0.25 \leq K_T < 0.35$ GeV/c
- $0.35 \leq K_T < 0.45$ GeV/c

4.1. Centrality and K_T Dependence of Correlation Function

From fig 4.1 and fig 4.2, it can be observed that for low centrality the CF is lowest and is highest for high centrality. This can be understand in connection with the source size. For low centrality, large radius of QGP is expected and small radius for high centrality. The low q width for the distribution of CF with q_{inv} with low centrality is less which implies the large radius of QGP from uncertainty principle and vice-versa. Similarly, from fig 4.3 and fig 4.4, it can be observed that CF with high K_T value has more q width which implies low source size from uncertainty principle and vice-versa. This is in very well agreement with what is expected theoretically.

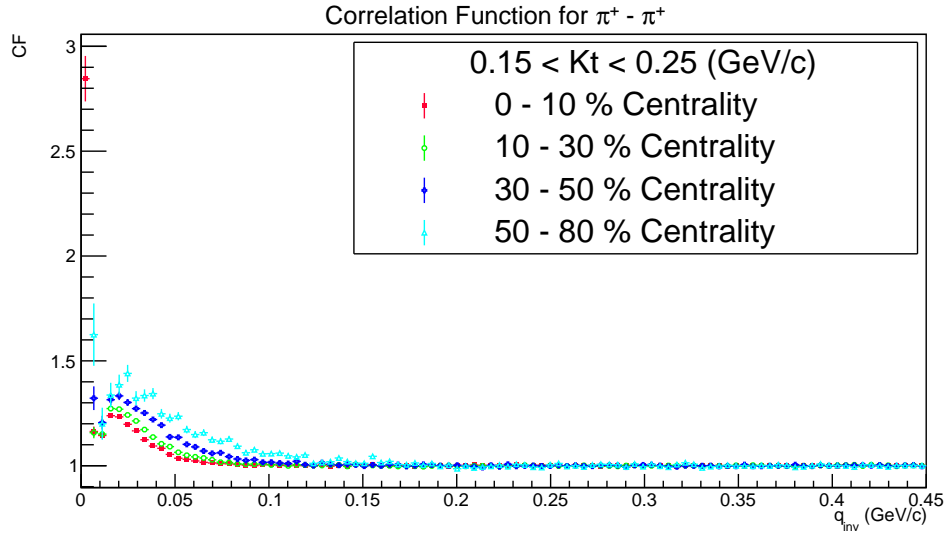


Figure 4.1: Correlation Functions for different ranges of centrality for K_T in [0.15,0.25) GeV/c for positive pions

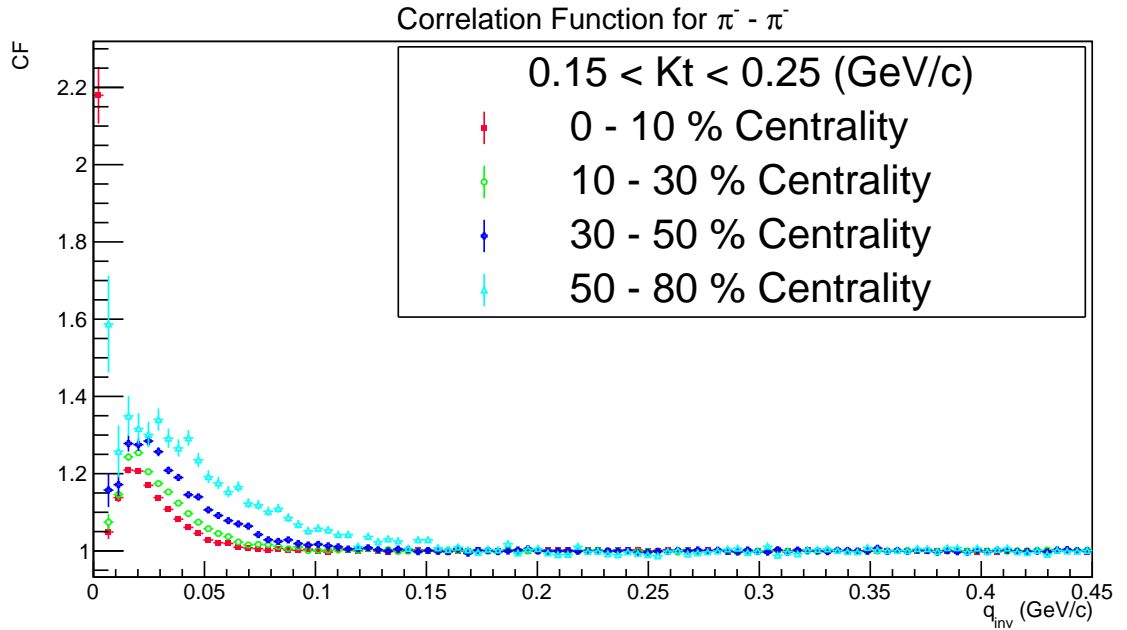


Figure 4.2: Correlation Functions for different ranges of centrality for K_T in [0.15,0.25) GeV/c for negative pions

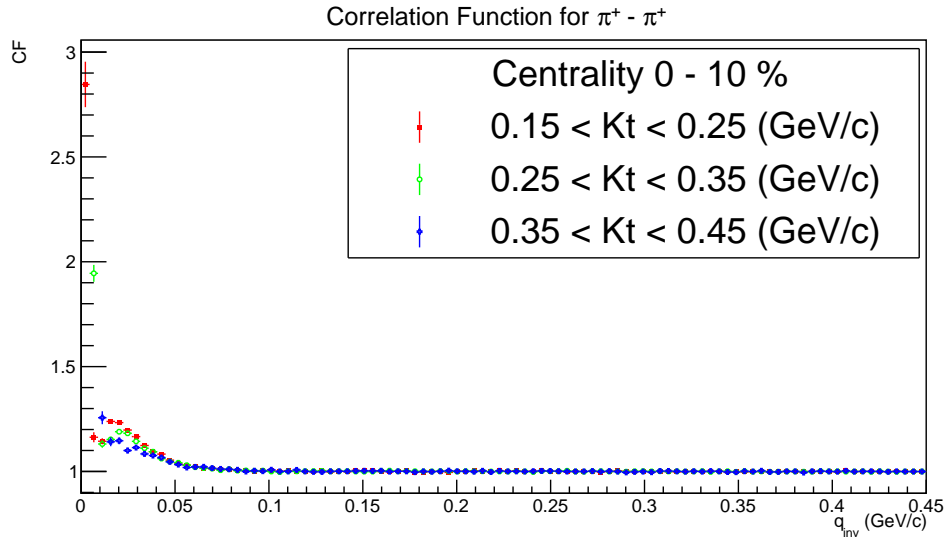


Figure 4.3: Correlation Functions for different ranges of K_T for 0 - 10 % centrality for positive pions

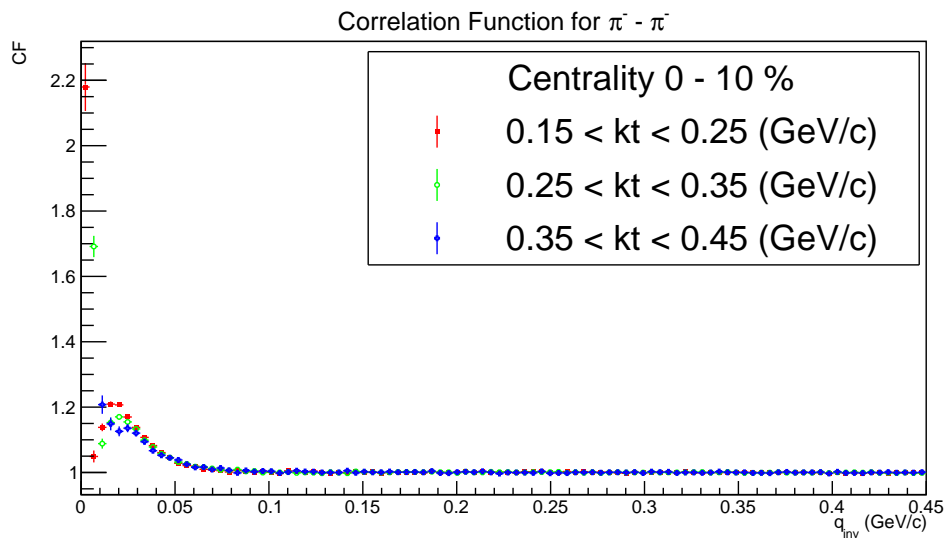


Figure 4.4: Correlation Functions for different ranges of K_T for 0 - 10 % centrality for negative pions

4.2. Dependence of CF on number of Vz bins

To check for the dependence of CF of number of Vz bins while mixing the events, the number of Vz bins have been taken to be 97, 58, 29, 19, 11, and 7. The correlation functions and their ratios with respect to the CF with 58 Vz bins while event mixing for positive and negative pions are plotted below.

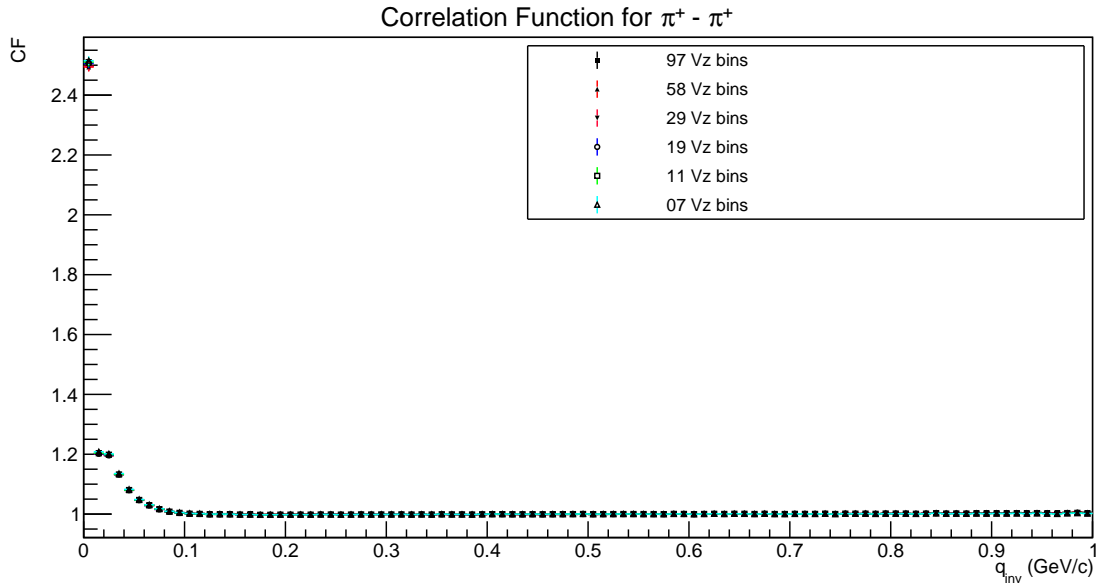


Figure 4.5: Correlation Functions with different Vz bins for event mixing for positive pions

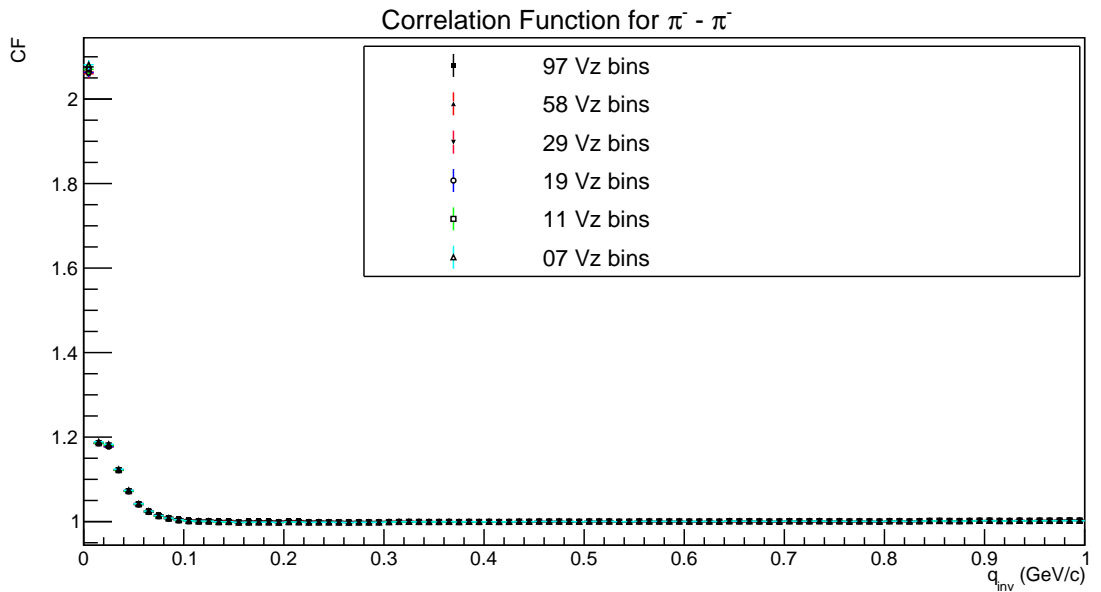


Figure 4.6: Correlation Functions with different Vz bins for event mixing for negative pions

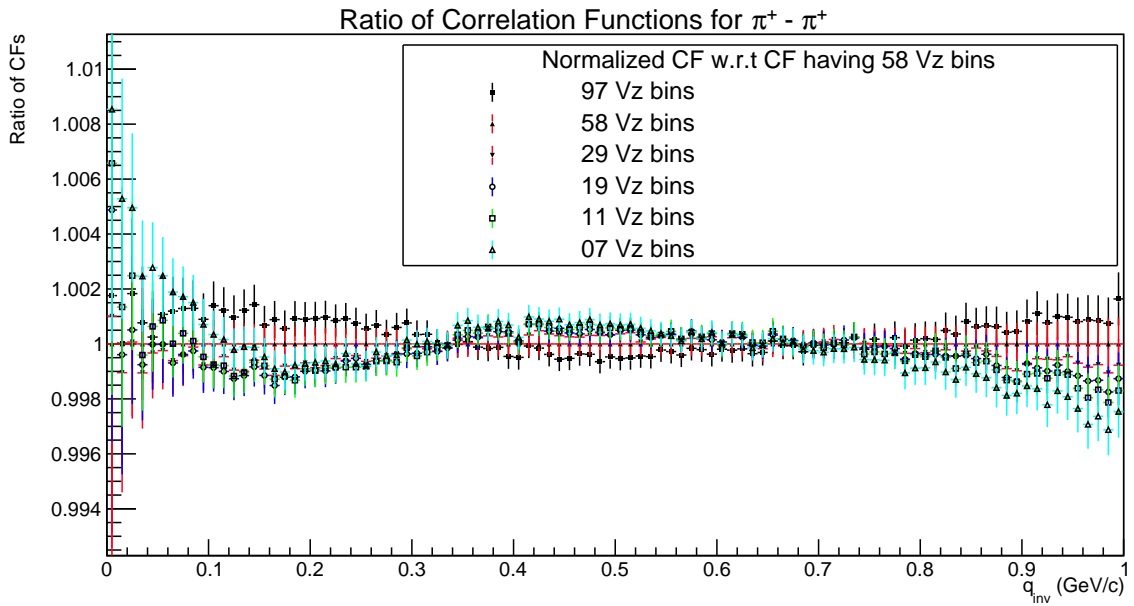


Figure 4.7: Ratio of CFs for different V_z bins w.r.t. CF with 58 V_z bins for event mixing for positive pions

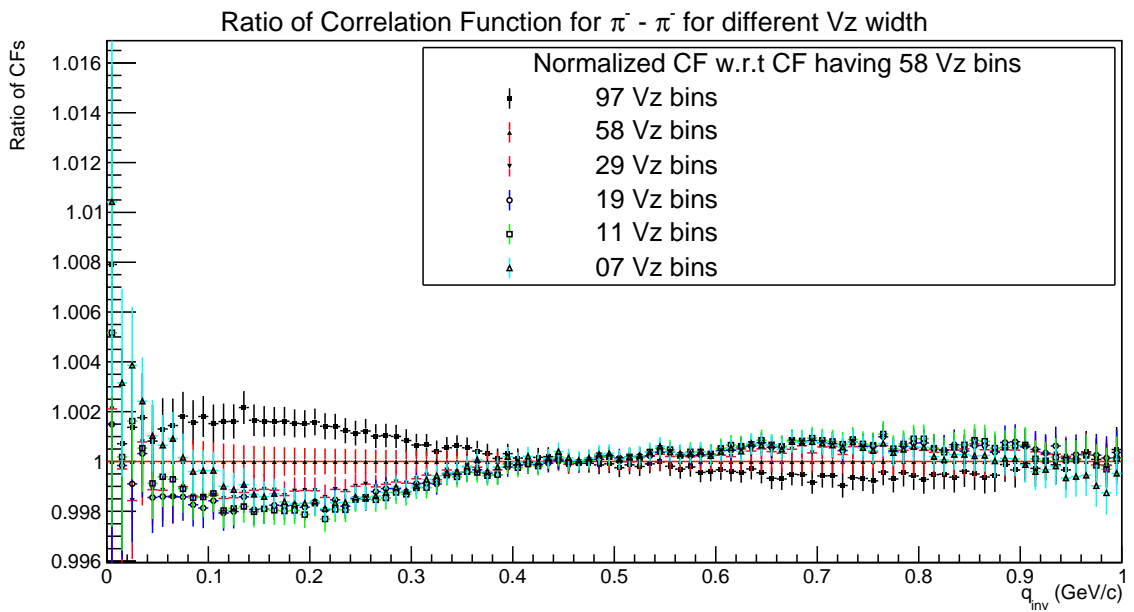


Figure 4.8: Ratio of CFs for different V_z bins w.r.t. CF with 58 V_z bins for event mixing for negative pions

From fig 4.5 and fig 4.6, there is not any significant difference could be noticed between the behavior of correlation functions when constructed by using different Vz width while mixing the events. For qualitative demonstration, the ratio plots is also plotted in fig 4.7 and fig 4.8. From the ratio plots, it can be seen that behavior of CF is opposite for Vz bins number greater than 58, than that of smaller than 58. At low q_{inv} values, the CF is higher for higher number of Vz bins upto 0.35 GeV/c for positive pions pair and 0.4 GeV/c for negative pions pair. After this range the CF with 97 Vz bins has become smallest for q_{inv} in approximately 0.38 to 0.6 GeV/c for positive pions and 0.45 to 0.85 GeV/c for negative pions. The exact reason for observed oscillation in behaviour of from these plots will require further analysis. However, it can be noticed that the fluctuation in correlation function with different Vz bins is within approximately 0.2% which will not cause any significant deviation in our results. Hence, we can claim that the effect of the correlation function on choosing Vz widths for event mixings is not statistically significant.

5. TRACK EFFECTS

Tracks can be merged or splitted during the reconstructions which will affect the behavior of correlation function specifically at low q values. Splitting tracks refers to the reconstruction of a single track as a pair of tracks, while merging tracks refers to the reconstruction of a pair of tracks as a single track. Each track is given a binary code that can be up to 72 bits (after recent iTPC upgrade) long (one bit for each pad), where 1 denotes the presence of a hit in this row of pads and 0 denotes its absence in order to properly divide tracks.

5.1. Splitting Level

When a single track is reconstructed as a pair of events, it would lead to increase in correlation functions. This effect can be clearly seen in the behavior of CFs at very q values which are plotted previously. To tackle this effect, we will defined the quantity Splitting Level (SL) as

$$SL = \frac{\sum S_i}{Nhits_{s_1} + Nhits_{s_2}},$$

where S_i is -1 if both the tracks have hit on the pad, 0 if none of the tracks have hit on the pad, and 1 if only one of the track has hit on the pad. $Nhits_{s_1} + Nhits_{s_2}$ are the total number of hits on pad of both tracks.

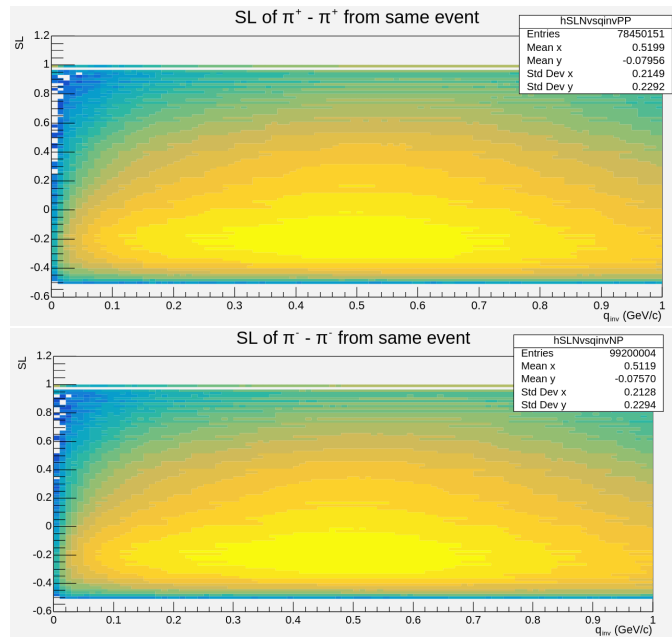


Figure 5.1: 2D plot of splitting level (SL) vs q_{inv} for positive pions and negative pions from same events.

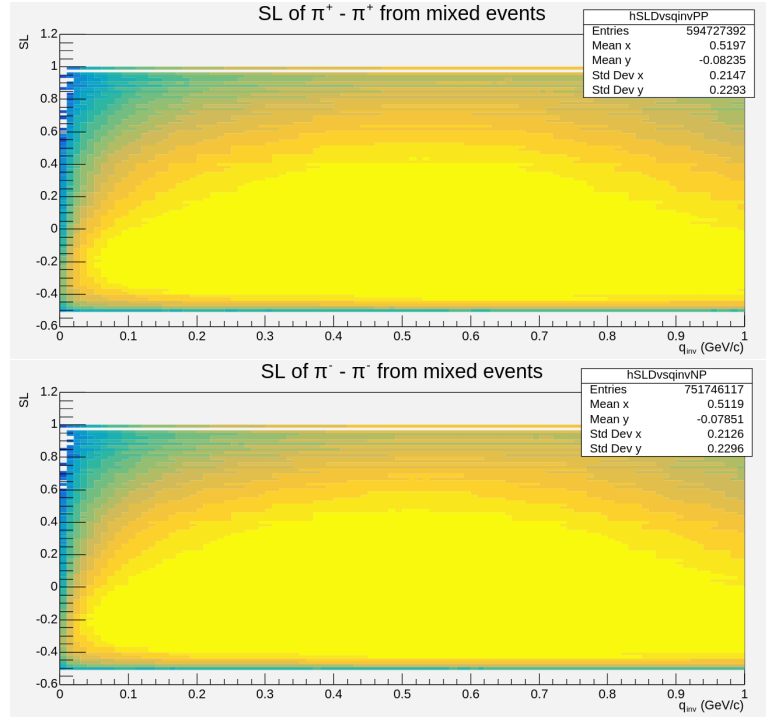


Figure 5.2: 2D plot of splitting level (SL) vs q_{inv} for positive pions and negative pions from mixed events.

Because of the definition of SL, it can take values between -0.5 to 1. -0.5 value of SL corresponds to case when both tracks have hit on the pad, 0 when no tracks have hit, and 1 if only one track has hit on the pad. Now, correlation function is plotted with different cuts on SL for the ranges of centrality and K_T to check for appropriate cuts to minimize the splitting events and maintaining the good statistics at the same time. Although the effect of splitting would be prominent in numerator of correlation function but will use this in both numerator and denominator for symmetry. From the above plots, it is clear the most of the data points are below the SL value of 0.4. Now, we will plot the correlation function for No SL cut and SL cuts of 0.8, 0.6, and 0.4 which is shown below.

The fig 5.3 and fig 5.4 represents the correlation function with different cuts on SL for different ranges of centrality and K_T for positive and negative pion pairs respectively. From the plots, we can see that for $SL < 0.6$, the correlation function is not changing much. Hence, the $SL < 0.6$ can be taken as a cut on splitting level.

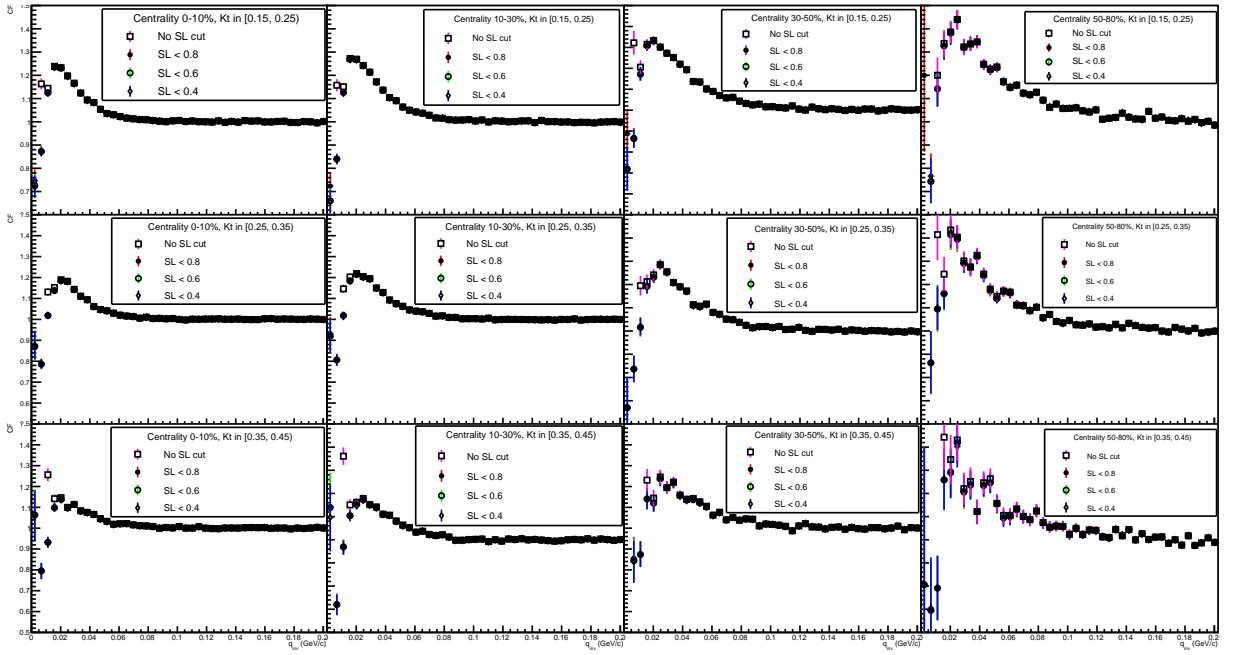


Figure 5.3: CF for different cuts on SL for different ranges of centrality and K_T for positive pions

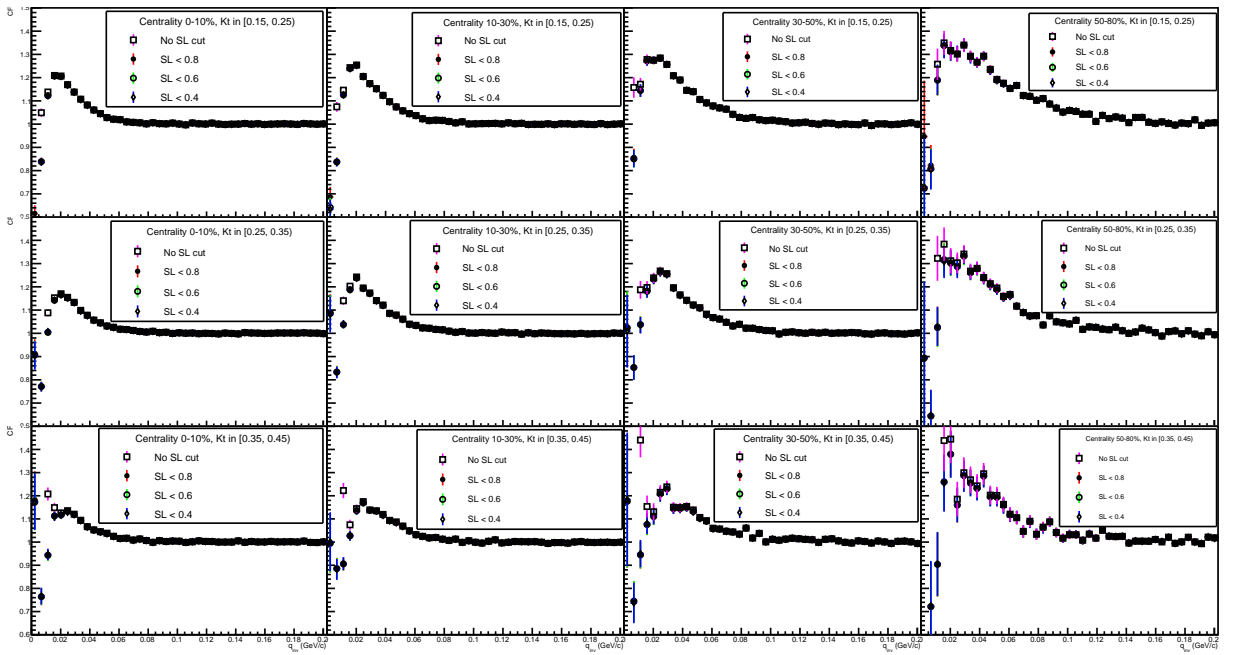


Figure 5.4: CF for different cuts on SL for different ranges of centrality and K_T for negative pions

5.2. Fraction of Merged Rows

Merging effect arises when a pair of tracks is constructed as a single tracks. This will reduce the value of correlation function. The fraction of merged rows (FMR) technique is employed in the current analysis to tackle this effect. It can take values from -1 to 1. It is defined by number of merged hits, which can be calculated by estimating the distance between the hit of one track to the hit of other track in the local TPC coordinate system. If this distance is smaller than the ionization cluster, then this will lead to the merged hits. The fraction of merged rows can be defined as

$$FMR = \frac{\text{No. of Merged Hits}}{\text{No. of rows where both track have a hit}}$$

where, the maximum number of TPC hits could be 72. The FMR value would be -1 if two tracks fall into different sectors of TPC as tracks falling on different sectors can not be merged.

Ideally, $FMR = -1$, would be the ideal case to eliminate the merging effects. But this could cause the loss of lots of statistics. So, the correlation function is studied with different cuts of FMR for the ranges of centrality and K_T in the quest of finding the optimized value of FMR. The cuts on FMR used in current analysis is 0.8, 0.6, 0.4, 0.2, 0.1, 0.05, and with no FMR cut.

Similar analysis is being used here from fig 5.9 and fig 5.10 for finding the cut in FMR as already did in for splitting levels. From the plots at low q_{inv} values, the splitting can be observed even among the FMR values of 0.1 and 0.05. Since, FMR value less than 0 (i.e., FMR value of -1) implies that tracks fall on different TPC sector and hence it would not cause the effect of merged hits. Hence, the FMR cut can be chosen to be less than 0.05.

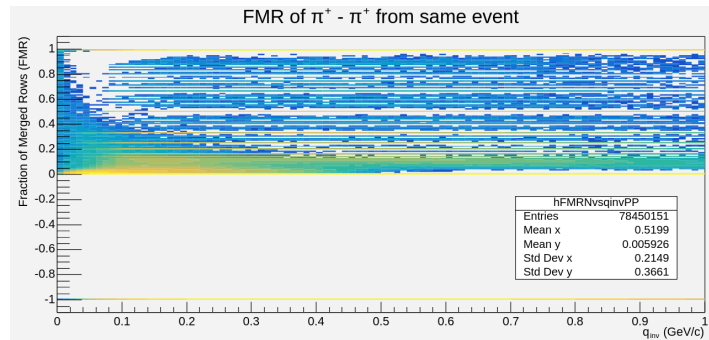


Figure 5.5: 2D plot of fraction of merged rows (FMR) vs q_{inv} for positive pions from same events.

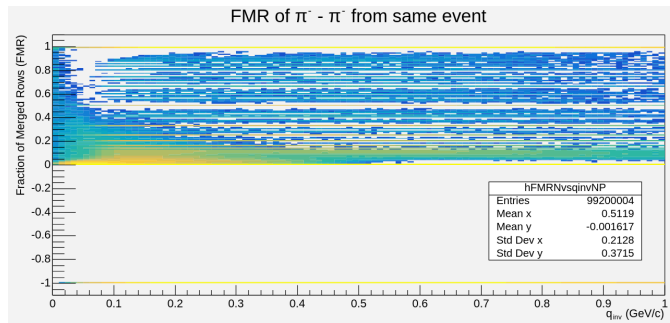


Figure 5.6: 2D plot of fraction of merged rows (FMR) vs q_{inv} for negative pions from same events.

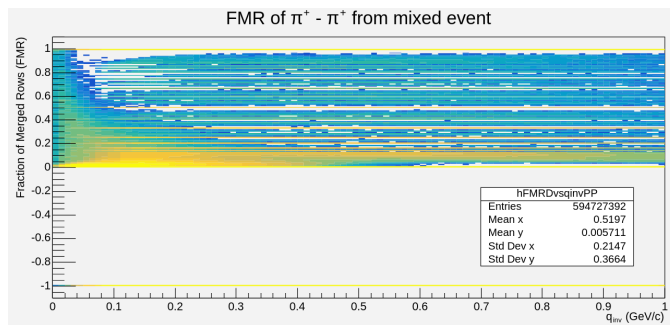


Figure 5.7: 2D plot of fraction of merged rows (FMR) vs q_{inv} for positive pions from mixed events.

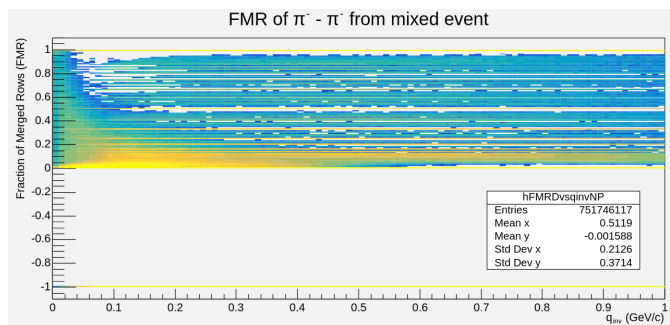


Figure 5.8: 2D plot of fraction of merged rows (FMR) vs q_{inv} for negative pions from mixed events.

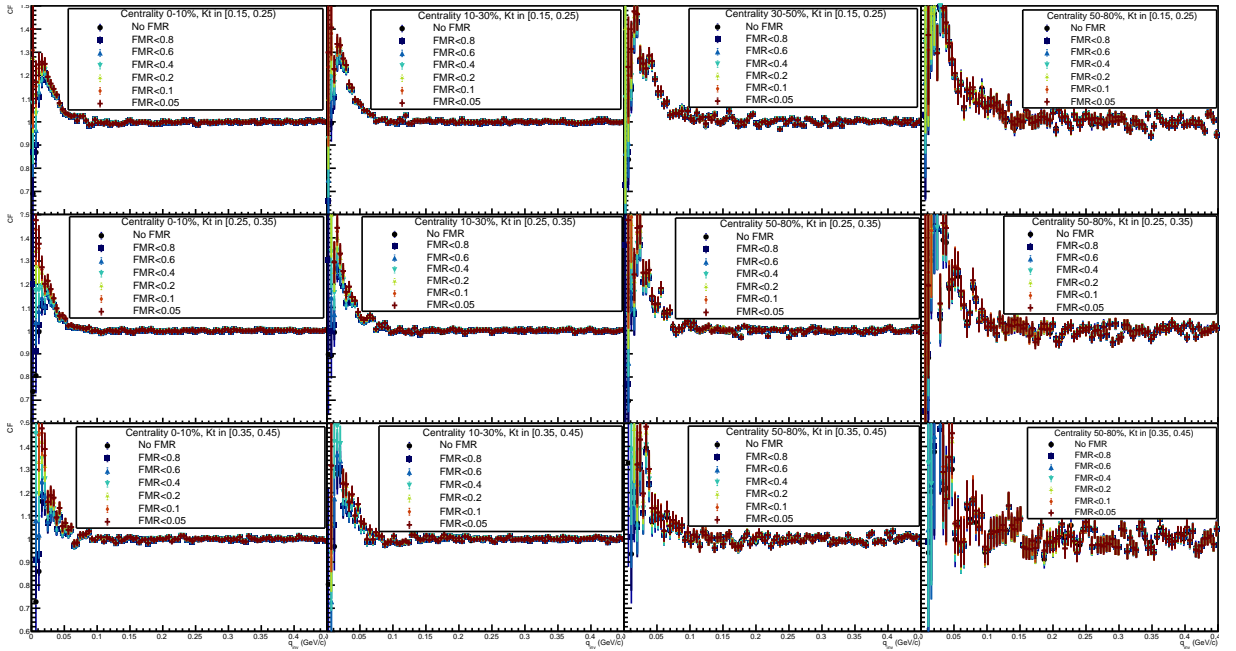


Figure 5.9: CF for different cuts on SL for different ranges of centrality and K_T for positive pions

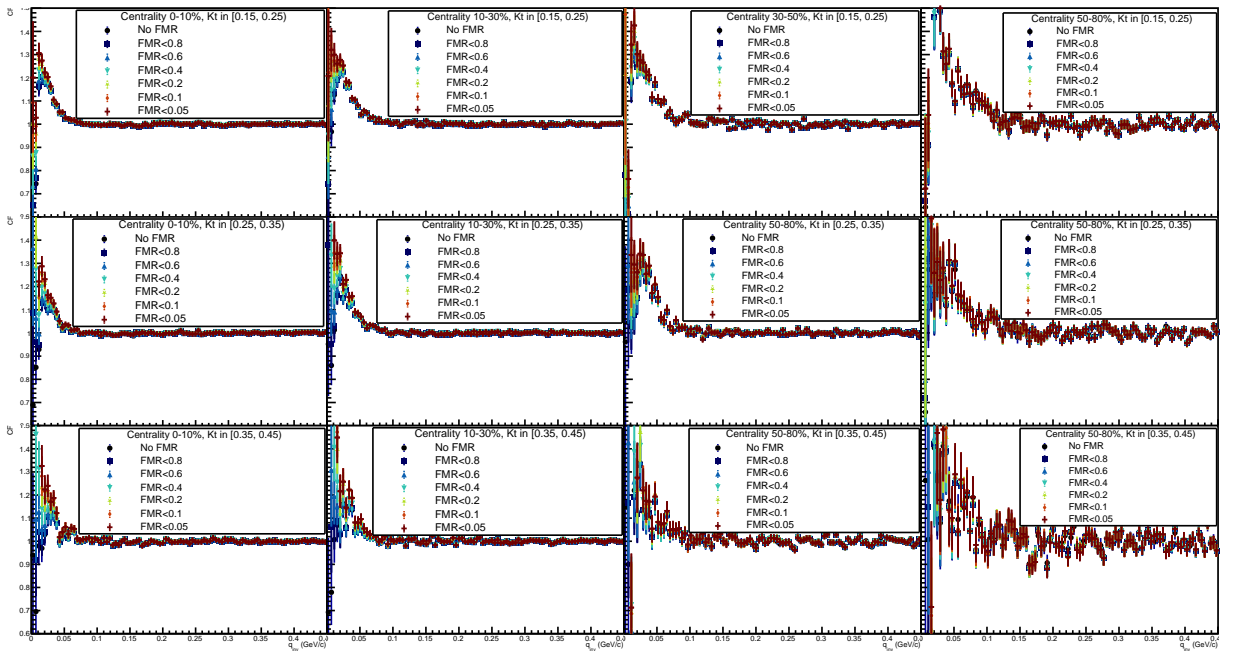


Figure 5.10: CF for different cuts on SL for different ranges of centrality and K_T for negative pions

6. ANALYSIS OF CORRELATION FUNCTION

6.1. Dependence of Correlation Function on V_z range

With the recent upgrade of iTPC, it is now possible to collect data from the the entire range of V_z of TPC i.e., -145 to 145 cm. It would be interesting to check if the correlation function can be build from the full V_z range of TPC. It would be equally interesting and important to check if there would be any dependence of correlation function on the chosen range of V_z for its construction. The analysis has been carried out initially at three ranges of V_z :

- -5 to 5 cm
- -80 to 80 cm
- -145 to 145 cm

In this kind of analysis, the width of V_z bin has been chosen to be 58 bins and will follow the same for rest of the analysis. The SL and FMR cuts of 0.6 and 0.05 respectively from the previous section has also been implemented for a good qualitative analysis of the CFs. The correlation function and their ratios for the above mentioned three V_z ranges has been plotted for positive and negative pion pairs in fig 6.1-6.4.

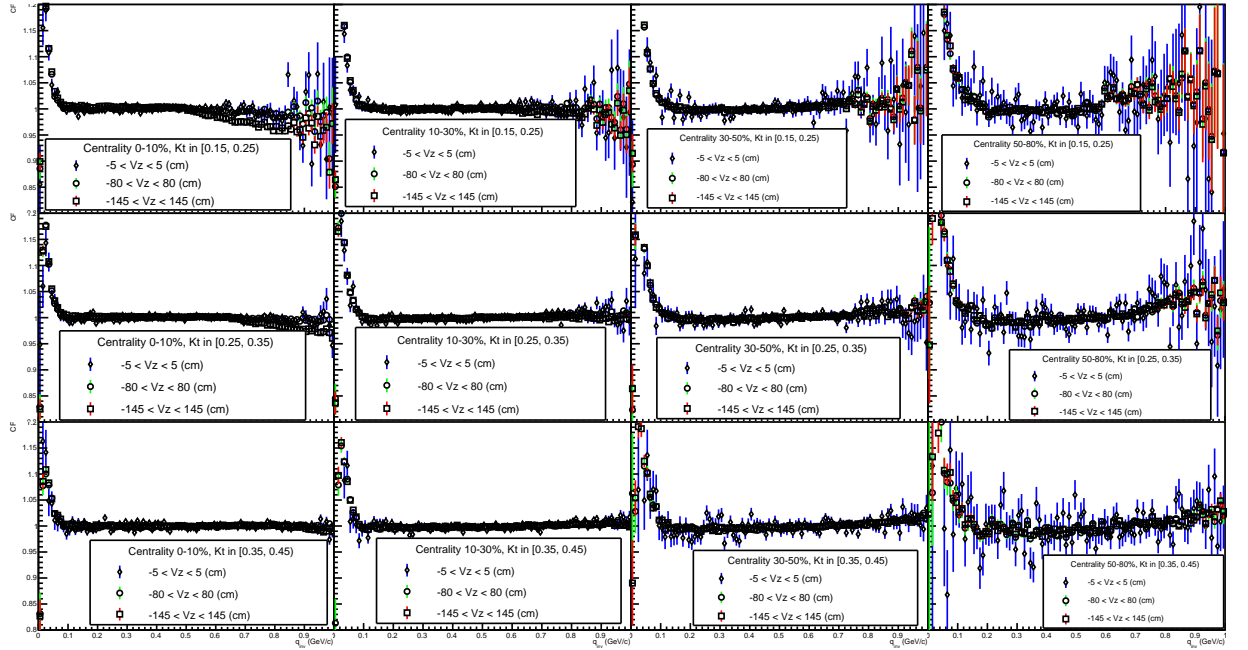


Figure 6.1: CF for positive pions with different ranges of V_z for different centrality and K_T range

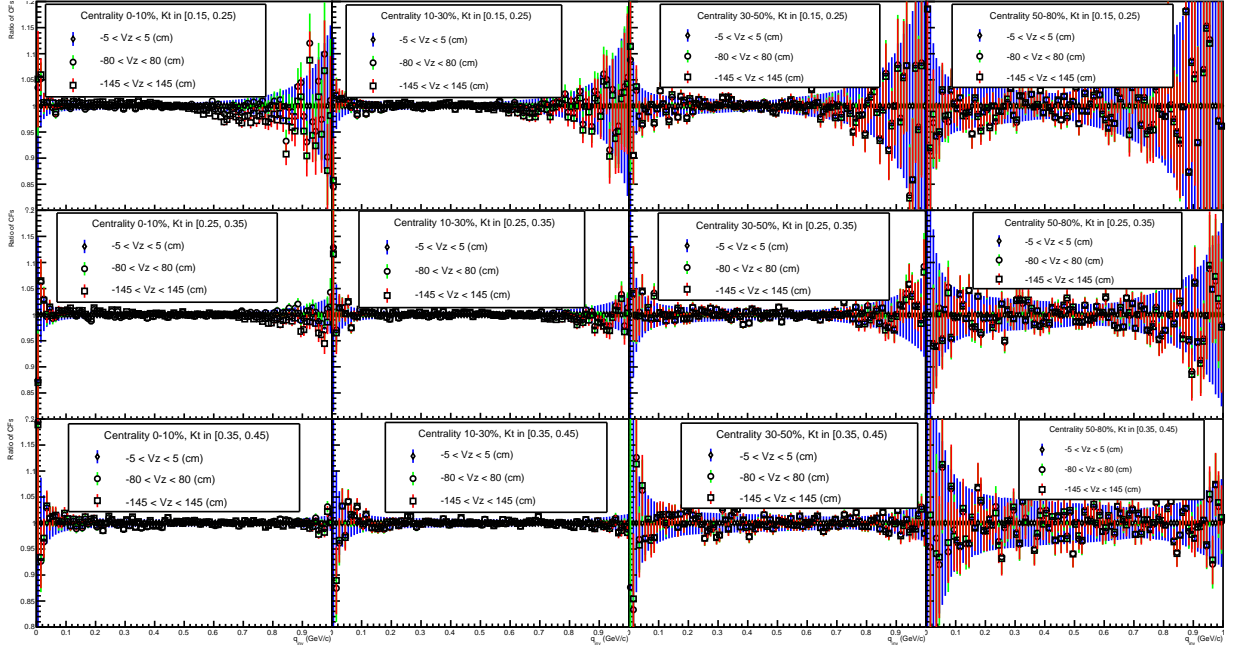


Figure 6.2: Ratio of CFs for positive pions with different ranges of V_z w.r.t CF in V_z range $(-5,5)$ cm for different centrality and K_T range

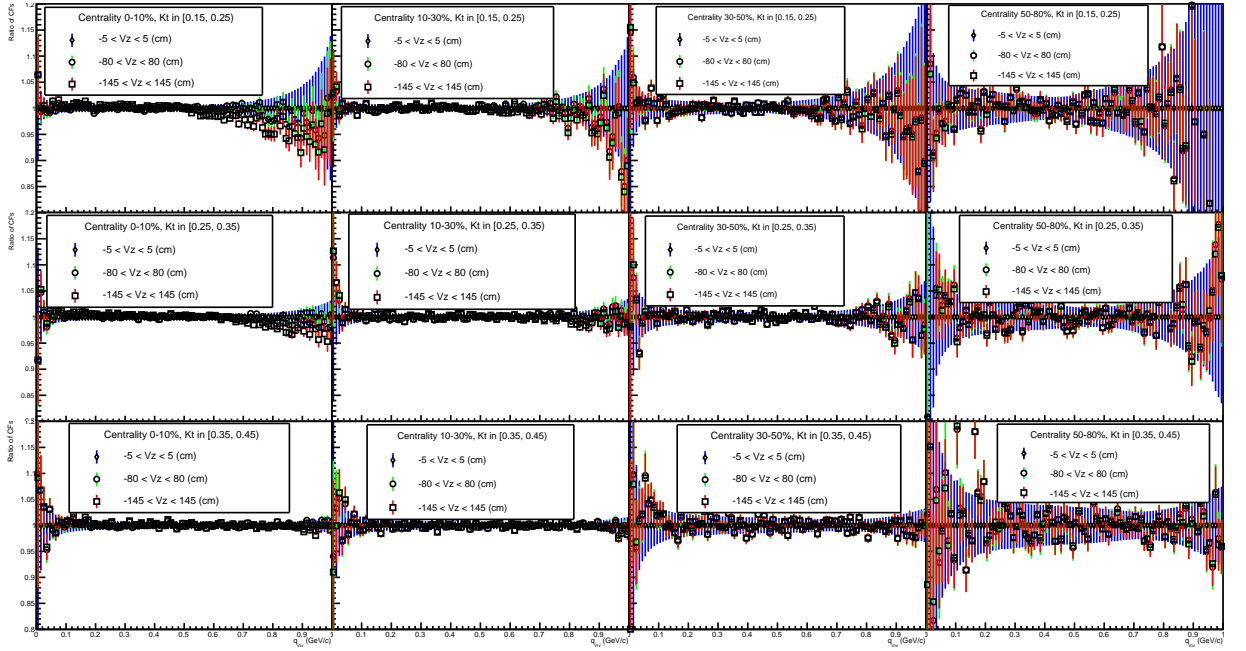


Figure 6.4: Ratio of CFs for negative pions with different ranges of V_z w.r.t CF in V_z range $(-5,5)$ cm for different centrality and K_T range

From the above plots, it can be noticed that the correlation function is quite same for all the three ranges of V_z . The fluctuations at higher q_{inv} value is also trivial in the plots with minimum K_T because of lack of significant data points in that regions. However, in the plots for centrality range 0-10% and K_T range 0.15-0.25, 0.25-0.35, the correlation function seems

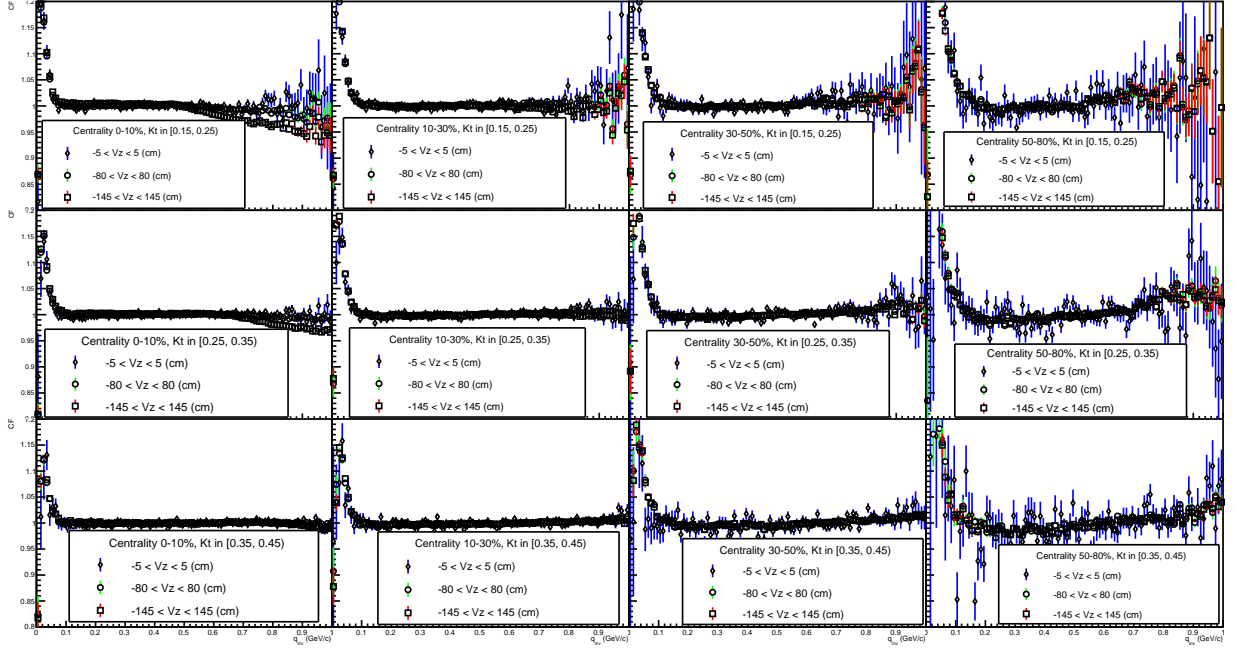


Figure 6.3: CF for negative pions with different ranges of V_z for different centrality and K_T range

to be decreasing for higher q_{inv} value. There are also error bars which are significant in that region which can be observed from ratio plots. To check for if it is just an statistical effects, the further analysis for both type of charges is carried out for V_z range:

- -145 to -115 cm
- -25 to 5 cm
- 5 to 35 cm
- 125 to 145 cm

From fig 6.5-6.8, it can be clearly seen that the lack of statistics for correlation function at higher q_{inv} for V_z in range -145 to -115 cm and 125 to 145 cm in the centrality range of 0-10%, and K_T in range 0.15-0.25 GeV/c and 0.25-0.35 GeV/c. This is causing a significant error bars in that region. So, it can be said that the fluctuation of correlation function for full V_z range at high q_{inv} mentioned above could be due to lack of statistics which would be causing the decrease in correlation function. But for low q_{inv} value (region which would be essential for fitting the correlation function), the correlation function is equally good even for higher V_z values as for the central V_z values. This is good success of recent iTPC upgrade and now the correlation function can be plotted even at the extreme values of V_z . From this

analysis, it can be concluded that the correlation function is independent of the V_z range chosen for analysis.

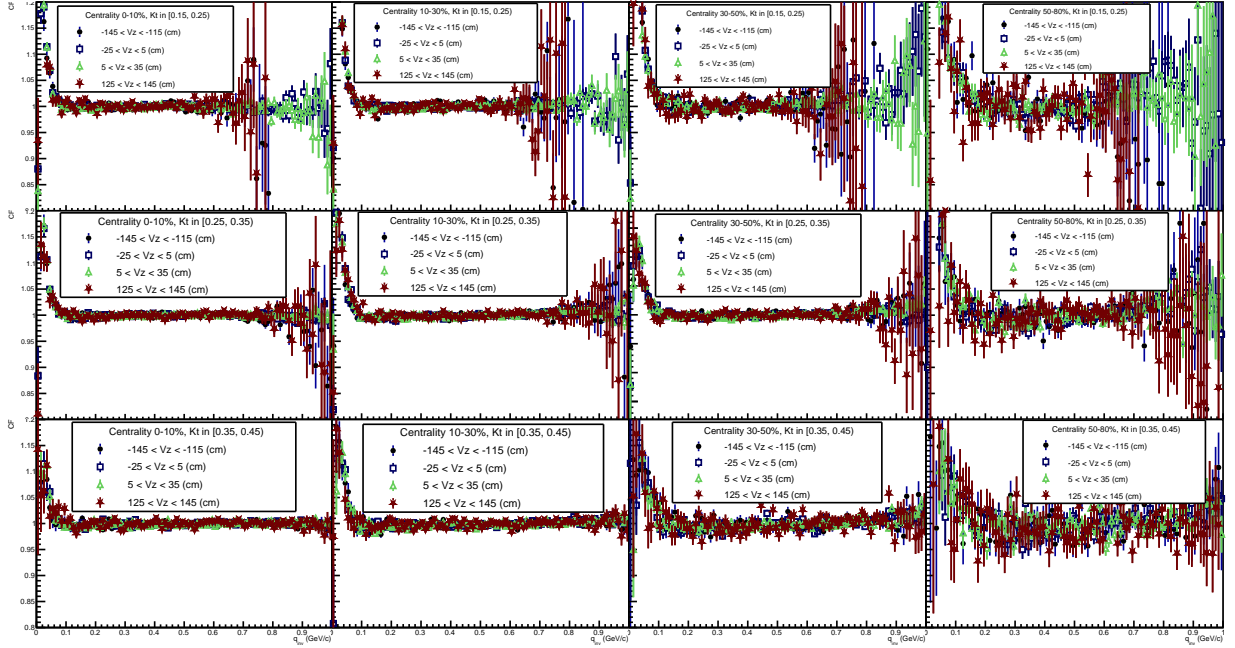


Figure 6.5: CF for positive pions with different ranges of V_z for different centrality and K_T range

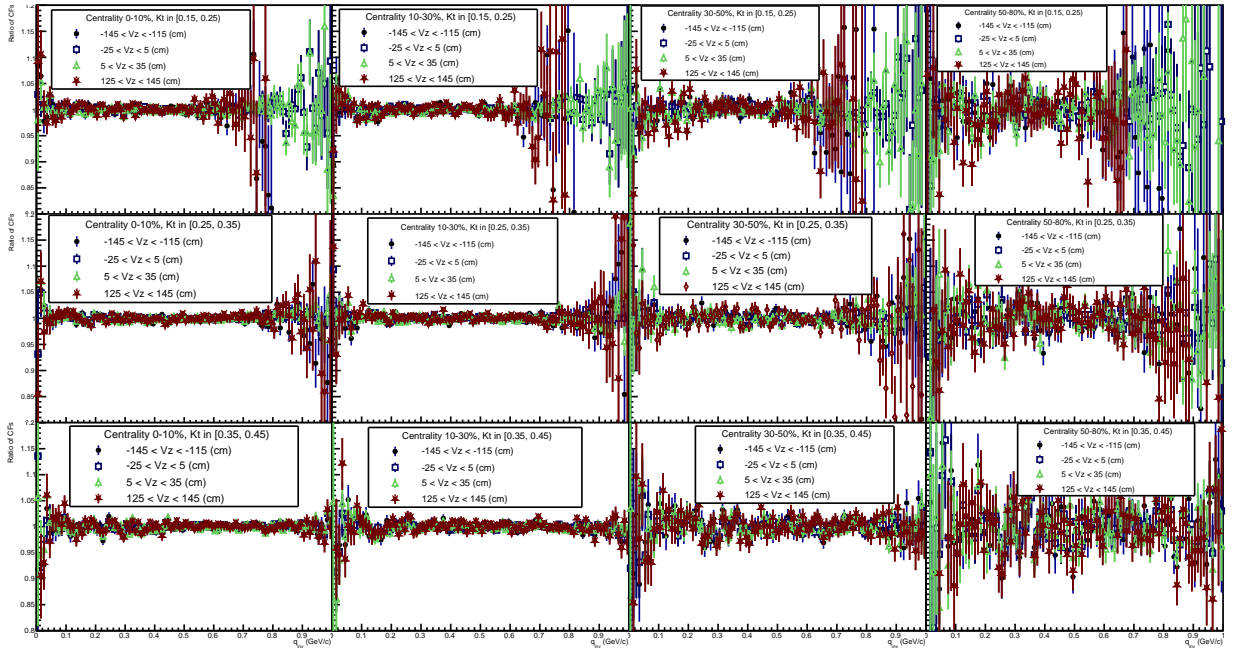


Figure 6.6: Ratio of CFs for positive pions with different ranges of V_z w.r.t CF in V_z range $(-5,5)$ cm for different centrality and K_T range

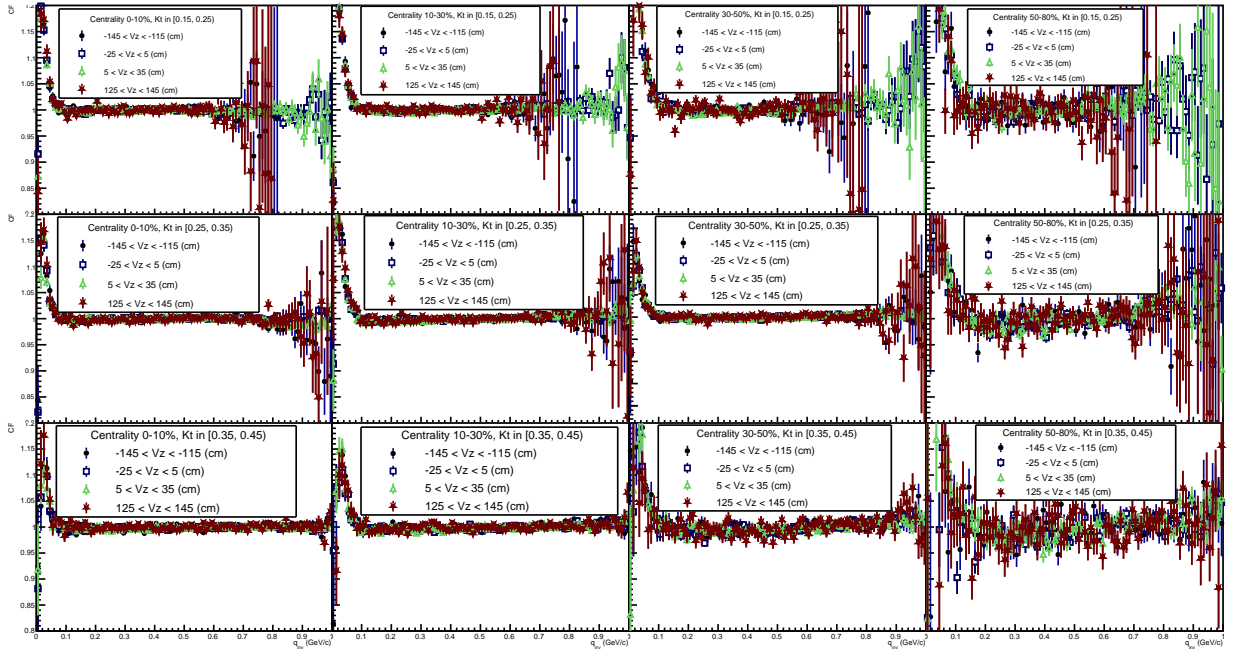


Figure 6.7: CF for negative pions with different ranges of V_z for different centrality and K_T range

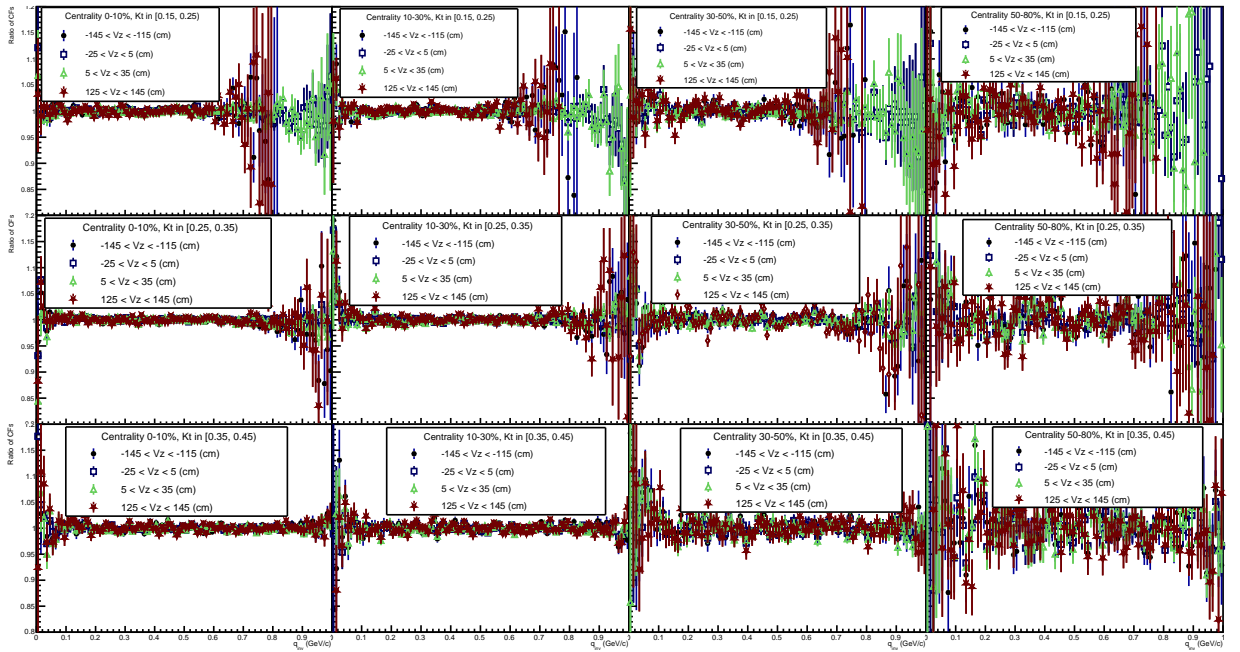


Figure 6.8: Ratio of CFs for negative pions with different ranges of V_z w.r.t CF in V_z range (-5,5) cm for different centrality and K_T range

6.2. Fitting of Correlation Function

The primary goal of the interferometry study of the pions is for finding the source size of the homogeneity region of the Quark-Gluon Plasma (QGP), which will be discussed in this section. The correlation function is fitted using the Bowler-Sinyukov function which can be represented as:

$$C(q) = (1 - \lambda) + \lambda K(q)(1 + e^{-q^2 R^2}),$$

where λ signifies the correlation strength between two particles, $K(q)$ is the coulombic correction, and R is the radius of the homogeneity region of the source. The Bowler-Sinyukov function is a fundamental theoretical tool utilized in particle physics for analyzing the correlations among particles emitted in heavy-ion collisions. This function serves as a fitting model to extract valuable information about the spatial and temporal properties of the particle-emitting source, offering insights into the source's size, shape, and dynamic behavior. Named after the physicists who proposed it, Bowler and Sinyukov, this function is designed to capture both the short-range and long-range correlations observed in particle correlations. It combines Gaussian and exponential terms, effectively encompassing the intricate interactions and dynamics of the particle-emitting system. The Gaussian term accounts for the initial interactions and conditions within the source, while the exponential term represents long-range correlations that can emerge due to collective motion and other phenomena.

By fitting the Bowler-Sinyukov function to experimental data, one can determine essential parameters such as the source's spatial radii and the strength of correlations among particles. This information provides critical insights into the particle source's behavior and the underlying physical processes governing the collision system.

The correlation function for both charges with $SL < 0.6$, and $FMR < 0.05$ has been fitted for the different ranges of centrality and K_T with the Bowler-Sinyukov function. The fitting parameters and χ^2/ndf value of the fit has also been reported.

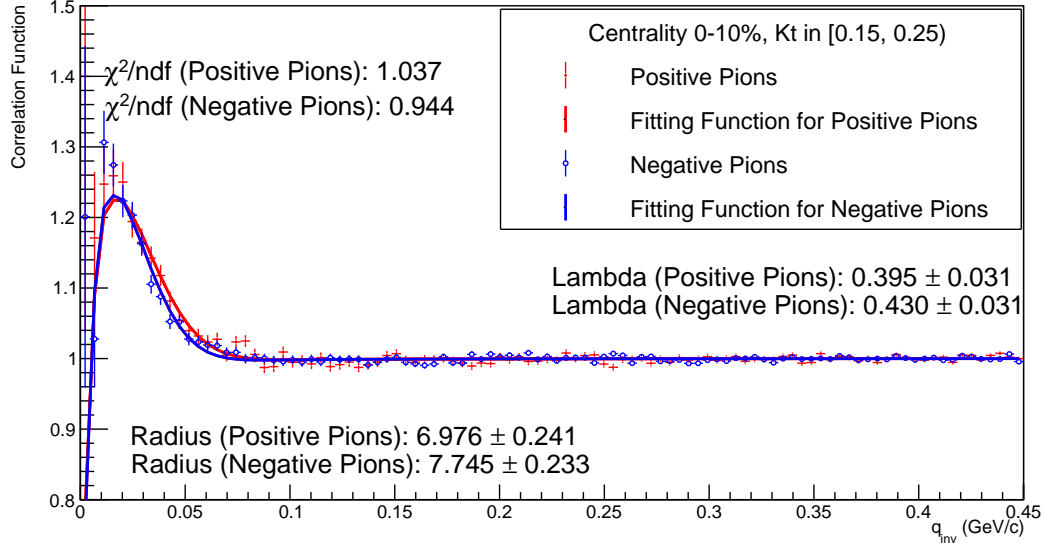


Figure 6.9: Fit of CF for positive and negative pion pairs for 0-10% centrality and $0.15 \leq K_T < 0.25$ GeV/c

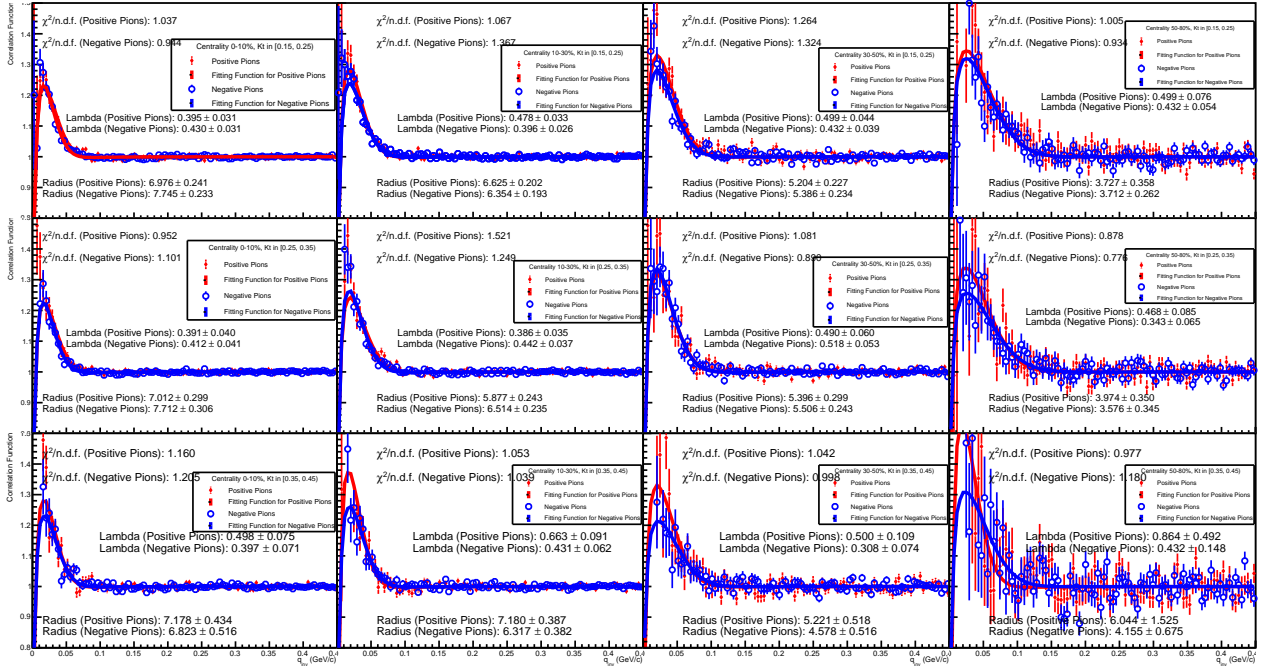


Figure 6.10: Fit of CF for positive and negative pion pairs for different ranges of centrality and K_T

It would also be interesting to visualize the behavior of radii and correlation strength of homogeneity region of the source with centrality. In fig 6.11, the R_{inv} is shown as a function of centrality for different charges in the K_T range of 0.15-0.25 GeV/c. It can be noticed the decrease in radii for both type of charges with increasing centrality. This is also what one can expect, i.e., the central collision will lead to larger source than the peripheral collision.

Similarly, from fig 6.12, the variation of correlation strength with centrality can be observed. It is interesting to notice the behavior of R_{inv} and λ for the most central centrals. The large difference in radii of homogeneity region for opposite charges could be due to third body effect. The word 'third body effect' here implies the interaction of pions with spectators and the source itself because of the low collision energy. The sudden decrease in correlation strength of positive pions for most central events could be due to resonance decays which would be very prominent for the most central events and the decrease in correlation strength of positive pions can be observed for most central events.

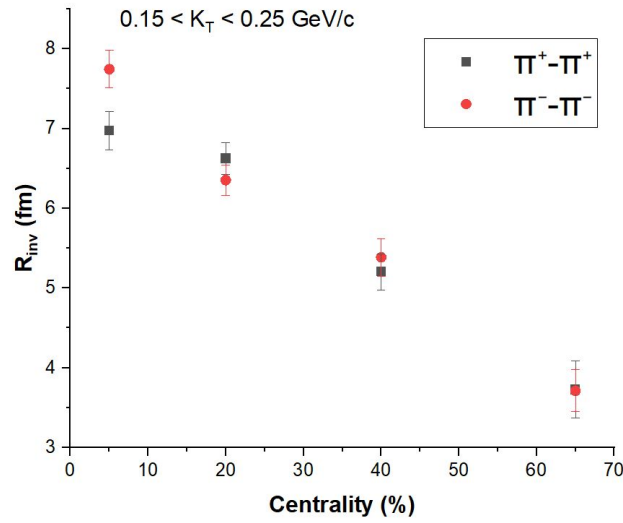


Figure 6.11: Radius of homogeneity region of the source for different charges as a function of centrality

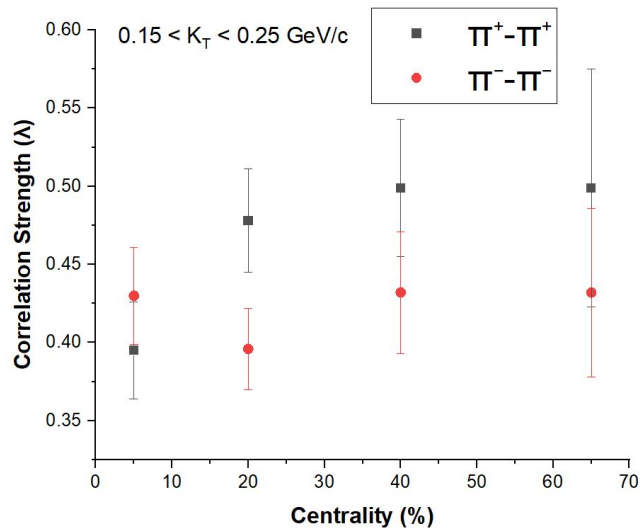


Figure 6.12: Variation of correlation strength (λ) with the centrality for different charges

7. CONCLUSION

Pion femtoscopy, a powerful technique for probing the spatial and temporal characteristics of particle-emitting sources, has played a pivotal role in advancing our understanding of heavy-ion collisions and the properties of the Quark-Gluon Plasma (QGP). Through the analysis of pion correlation functions, one gains insights into the size, shape, and dynamics of the source, shedding light on the intricate nature of particle interactions and the evolution of the early universe. In this context, the Bowler-Sinyukov function, a theoretical model, has proven to be a valuable tool for fitting correlation functions and extracting meaningful physical parameters. This conclusion encapsulates the significance and achievements of pion femtoscopy analysis while emphasizing the merits of using the Bowler-Sinyukov function for this purpose.

Pion femtoscopy analysis has revolutionized our ability to decipher the secrets of particle-emitting sources in heavy-ion collisions. By exploiting the correlations between pion pairs, this technique enables us to uncover the spatial dimensions of the particle source and investigate the effects of collective motion and interactions. The information extracted from pion correlation functions transcends mere numerical values; it provides us with a vivid picture of the conditions prevailing during the early stages of the universe's evolution. The size and shape of the particle-emitting source offer insights into the expansion dynamics, the role of hydrodynamic flow, and the interplay of quantum statistics.

The construction of the correlation function entails a critical step, which involves the amalgamation of pion pairs originating from different events. This pivotal process revolves around the discernment of the most pertinent events to be combined, ultimately forming the background reference. This selection process is meticulously conducted by opting for events characterized by comparable multiplicities and originating from analogous V_z ranges. It is worth noting that the manner in which this background is established can potentially influence the behavior of the correlation function.

It is imperative to ascertain the correlation function's sensitivity to the number of V_z (vertex position along the beam axis) bins utilized in the event mixing procedure. A comprehensive investigation has been conducted to analyze this dependency, ultimately culminating in the confirmation of the correlation function's robust independence from the number of V_z bins employed for event mixing. This assurance underscores the reliability of the methodology and ensures that the correlation function remains consistent across varying V_z bin numbers.

Additionally, a thorough exploration has been undertaken to evaluate the correlation func-

tion's susceptibility to alterations in the V_z range. This systematic inquiry has led to the resolute determination that the correlation function exhibits steadfast independence from changes in the V_z range. This validation underscores the methodological rigor and solidifies the reliability of the correlation function, irrespective of shifts in the considered V_z span.

The process of constructing the correlation function entails meticulous event selection for the purpose of forming a background reference. The selection criteria encompass similar event multiplicities and akin V_z ranges. Moreover, investigations into the correlation function's responsiveness to variations in the number of V_z bins and V_z range have yielded robust findings, affirming the correlation function's stability and steadfastness across these parameters. This comprehensive evaluation contributes to the integrity and credibility of recent iTPC upgrade of STAR detector.

Pion femtoscopy analysis, supported by the fitting capabilities of the Bowler-Sinyukov function, has contributed immensely to our understanding of the Quark-Gluon Plasma and its behavior during heavy-ion collisions. The ability to discriminate between different stages of the collision process and to deduce the evolution of the QGP medium is instrumental in verifying theoretical models and refining our understanding of the strong force and the fundamental nature of matter. Beyond the realm of particle physics, the insights gained from pion femtoscopy analysis have implications for cosmology, astrophysics, and our comprehension of the early universe.

The application of the Bowler-Sinyukov function to pion femtoscopy analysis has yielded significant achievements. By fitting this model to experimental correlation data, parameters such as the source size, and the correlation strength have successfully extracted. These parameters carry essential information about the particle-emitting source and the dynamics of particle production. The Bowler-Sinyukov function's ability to capture both short-range and long-range correlations has led to improved accuracy in fitting and a more holistic understanding of the source properties. The dependence of these parameters on the centrality also reflected the presence of third body effect for highly central events which could have been expected because of low collision energy.

While the Bowler-Sinyukov function has proven its efficacy, challenges remain in pion femtoscopy analysis. These include the accurate treatment of experimental effects, the influence of resonance decays, and the consideration of multi-particle emission sources. Future directions should focus on refining theoretical models, enhancing experimental techniques, and exploring alternative fitting functions to achieve even greater precision in characterizing particle-emitting sources.

In conclusion, pion femtoscopy analysis, facilitated by the fitting of correlation functions

using the Bowler-Sinyukov function, stands as a cornerstone in our quest to understand the universe's fundamental building blocks and its early evolution. This synergy of theoretical insight and experimental exploration has allowed us to peer into the intricate dynamics of particle interactions, offering a glimpse into the conditions that prevailed during the formative stages of the cosmos. As technology advances and our understanding deepens, the journey of pion femtoscopy continues to illuminate the path towards a more comprehensive understanding of the universe's origins and the forces that shape its destiny.

References

- [1] Adams J., Aggarwal M. M., Ahammed Z., Amonett J., Anderson B. D., Arkhipkin D., Averichev G. S., et al., 2005, *PhRvC*, 71, 044906. doi:10.1103/PhysRevC.71.044906
- [2] Kraeva A., STAR Collaboration, 2022, *PAN*, 85, 988. doi:10.1134/S1063778823010313
- [3] Anson C. D., 2014, PhDT
- [4] Akkelin S. V., Sinyukov Y. M., 1995, *PhLB*, 356, 525. doi:10.1016/0370-2693(95)00765-D
- [5] Annan Lisa M., Pratt S., Soltz R., Wiedemann U., 2005, *ARNPS*, 55, 357. doi:10.1146/annurev.nucl.55.090704.151533
- [6] Barrette, J., Bellwied, R., Bennett, S., Braun-Munzinger, P., Chang, W.C., Cleland, W.E., and, ...: 1997, *Physical Review C* **55**, 1420. doi:10.1103/PhysRevC.55.1420.
- [7] Bowler M. G., 1988, *ZPhyC*, 39, 81. doi:10.1007/BF01560395
- [8] Goldhaber G., Fowler W. B., Goldhaber S., Hoang T. F., Kalogeropoulos T. E., Powell W. M., 1959, *PhRvL*, 3, 181. doi:10.1103/PhysRevLett.3.181
- [9] Goldhaber G., Goldhaber S., Lee W., Pais A., 1960, *PhRv*, 120, 300. doi:10.1103/PhysRev.120.300
- [10] Pratt S., 1984, *PhRvL*, 53, 1219. doi:10.1103/PhysRevLett.53.1219
- [11] Sinyukov Y. M., Lednický R., Akkelin S. V., Pluta J., Erasmus B., 1998, *PhLB*, 432, 248. doi:10.1016/S0370-2693(98)00653-4
- [12] G. Nigmatkulov [STAR], *KnE Energ. Phys.* **3** (2018), 286-290 doi:10.18502/ken.v3i1.1756 [arXiv:1712.09964 [nucl-ex]].
- [13] J. S. Nico and W. M. Snow, *Ann. Rev. Nucl. Part. Sci.* **55** (2005), 27-69 doi:10.1146/annurev.nucl.55.090704.151611 [arXiv:nucl-ex/0612022 [nucl-ex]].
- [14] S. Acharya *et al.* [ALICE], *Phys. Rev. C* **96** (2017) no.6, 064613 doi:10.1103/PhysRevC.96.064613 [arXiv:1709.01731 [nucl-ex]].
- [15] M. Anderson, J. Berkovitz, W. Betts, R. Bossingham, F. Bieser, R. Brown, M. Burks, M. Calderon de la Barca Sanchez, D. A. Cebra and M. G. Cherney, *et al.* *Nucl. Instrum. Meth. A* **499** (2003), 659-678 doi:10.1016/S0168-9002(02)01964-2 [arXiv:nucl-ex/0301015 [nucl-ex]].

A. APPENDIX

In this section, the plots for various cuts used for event and track selection and before and after particle identification has been shown. The left side of plot represents the scenario before applying any constraint, and right side is the representation of changes after putting the required constraints. The exact values of cuts has been already discussed in Chapter 3.

A.1. Event Selection

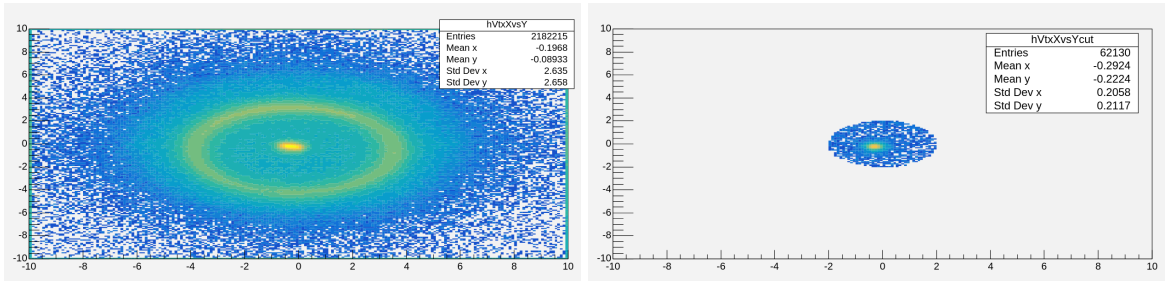


Figure A.1: The radial distribution of vertex position before and after the cut $V_r < 2$ cm

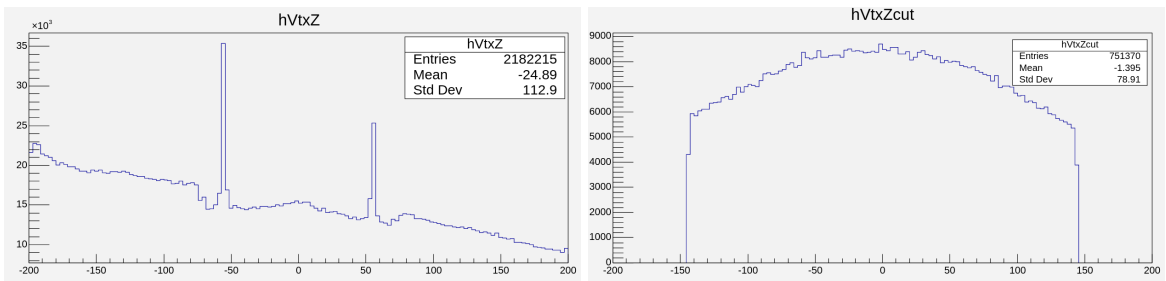


Figure A.2: Plot of vertex position in z-direction before and after the cut $|v_z| < 145$ cm

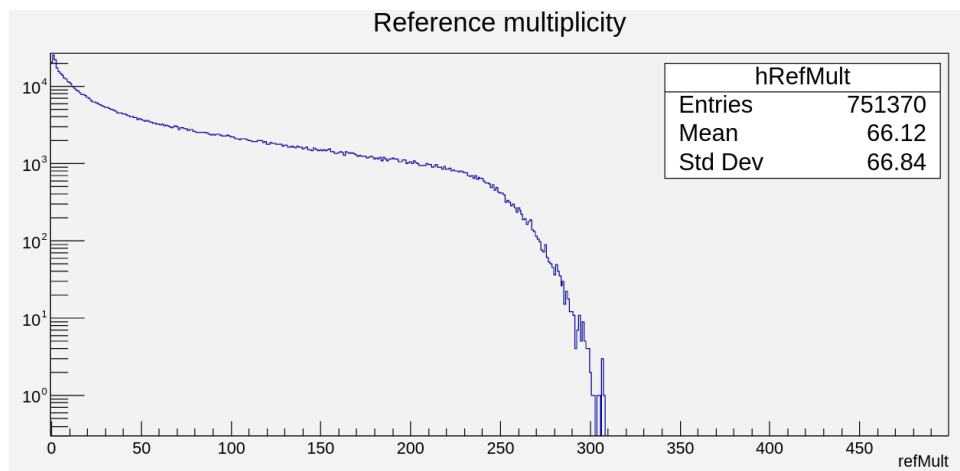


Figure A.3: Reference Multiplicity after Event Selection

A.2. Track Selection

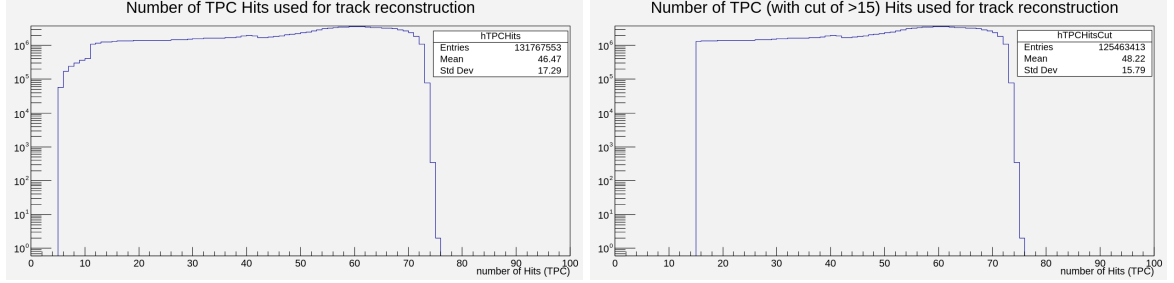


Figure A.4: Number of TPC hits used for track reconstruction before and after the cut

$$N_{hits}^{fits} \geq 15$$

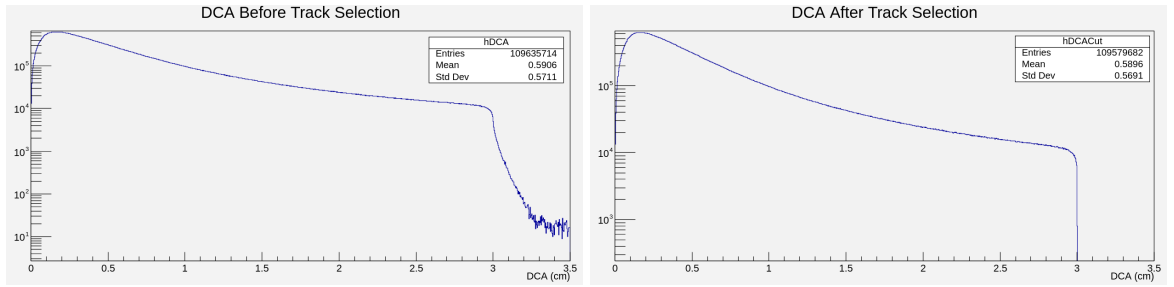


Figure A.5: Distance of closed approach (DCA) before and after the track selection

$$(|DCA| < 3 \text{ cm})$$

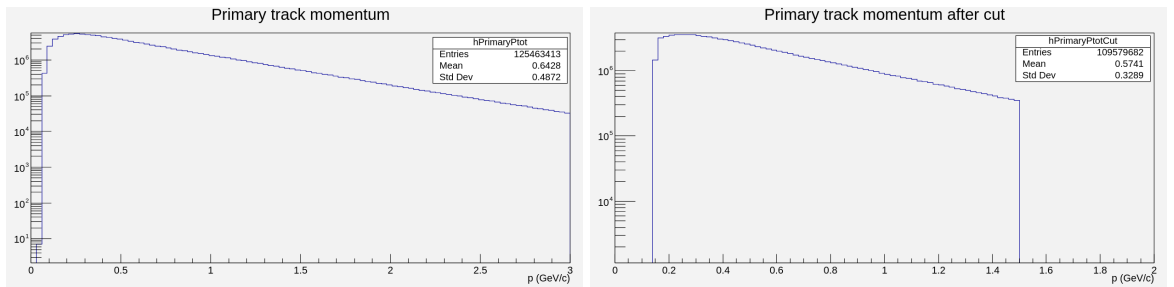


Figure A.6: Distribution of total momentum of primary track before and after the cut of

$$0.15 < p_{tot}^{prim} < 1.5 \text{ GeV}/c$$

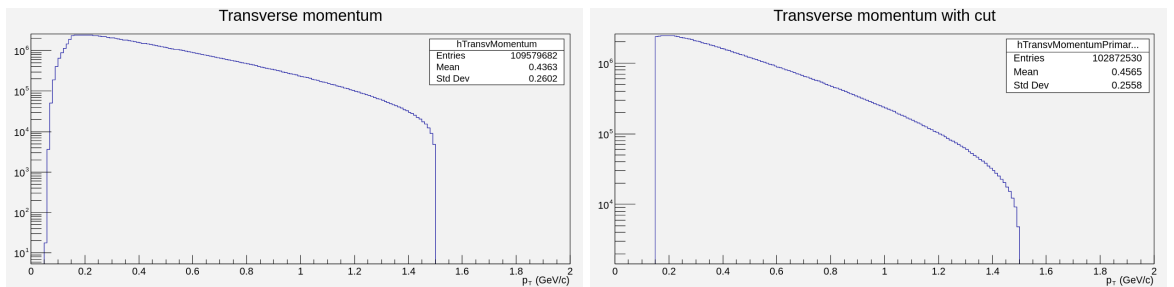


Figure A.7: Distribution of transverse momentum of primary track before and after the cut

$$\text{of } 0.15 < p_T^{prim} < 1.5 \text{ GeV}/c$$

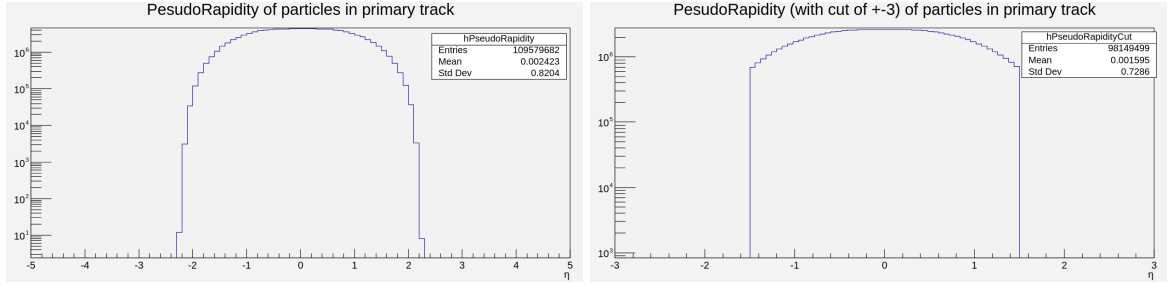


Figure A.8: Distribution of pseudorapidity before and after the cut $|\eta| < 1.5$

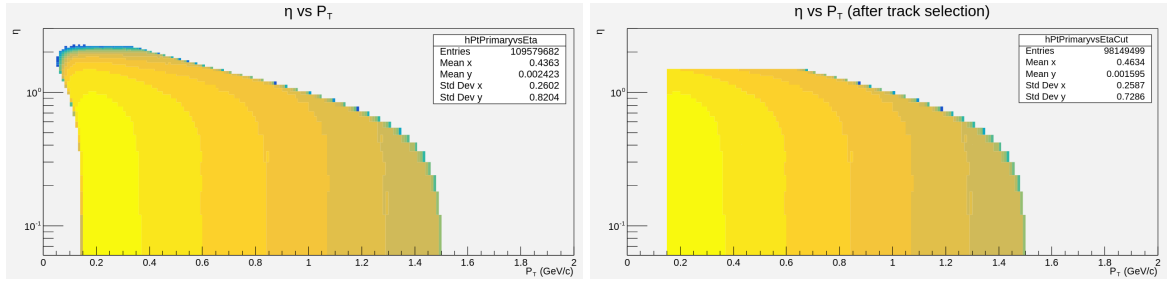


Figure A.9: Distribution of pseudorapidity as a function of transverse momentum before and after the cut for track selection

A.3. Particle Identification

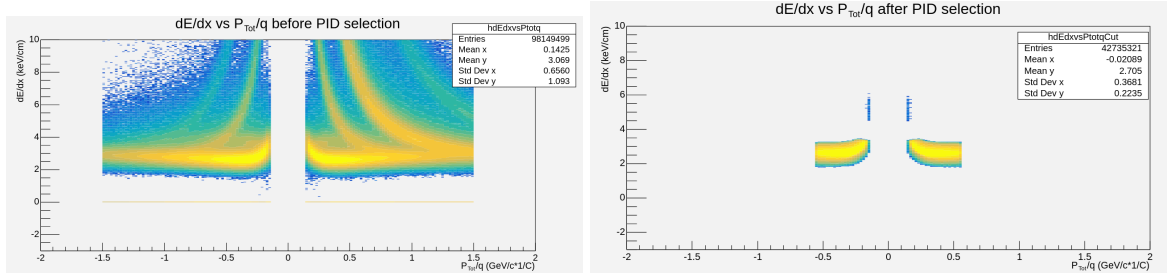


Figure A.10: The distribution of dE/dx with p_{tot}^{prim} before and after PID

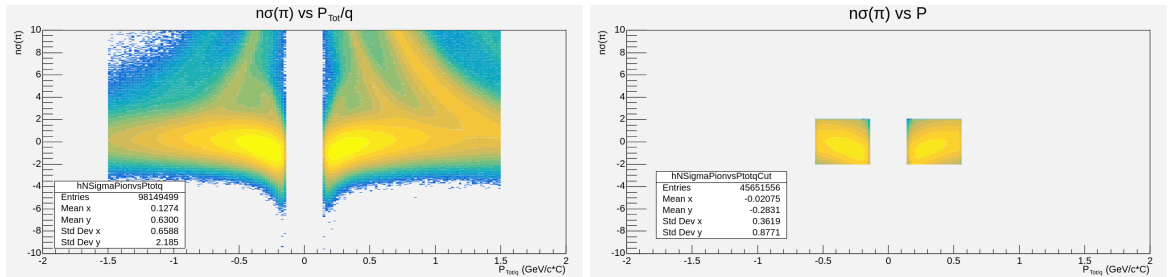


Figure A.11: $n\sigma(\pi)$ distribution before and after the cut $|n\sigma(\pi)| < 2$

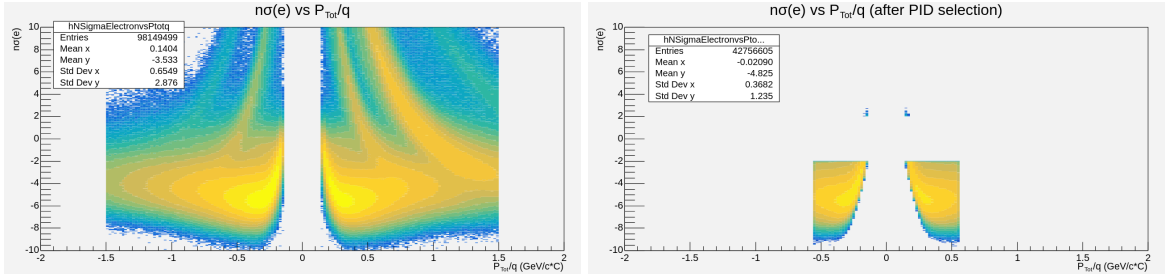


Figure A.12: $n\sigma(e)$ distribution before and after the cut $|n\sigma(e)| > 2$

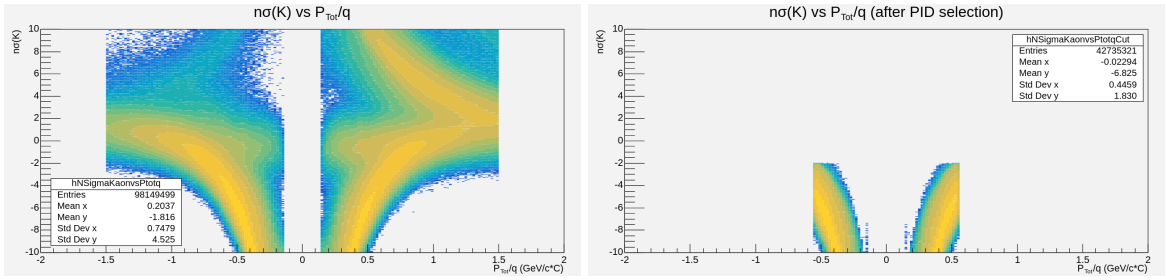


Figure A.13: $n\sigma(K)$ distribution before and after the cut $|n\sigma(K)| > 2$

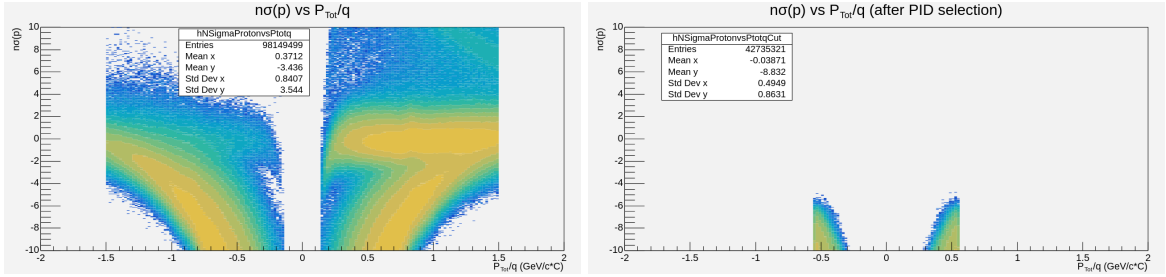


Figure A.14: $n\sigma(p)$ distribution before and after the cut $|n\sigma(p)| > 2$

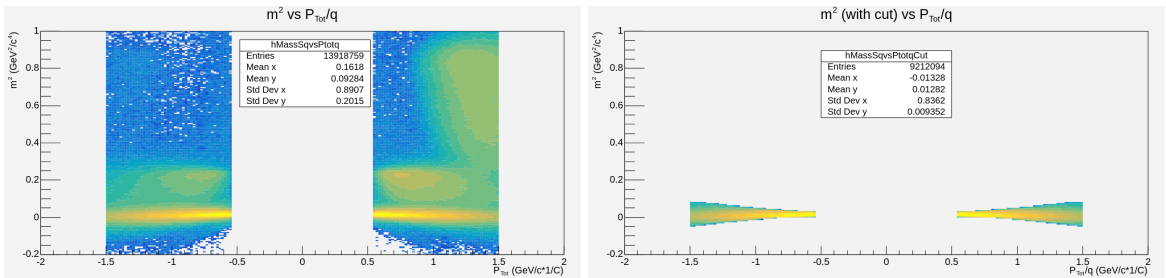


Figure A.15: The distribution of m^2 of pions before and after the cut $-0.05 < m^2 < 0.08 \text{ GeV}^2/c^4$

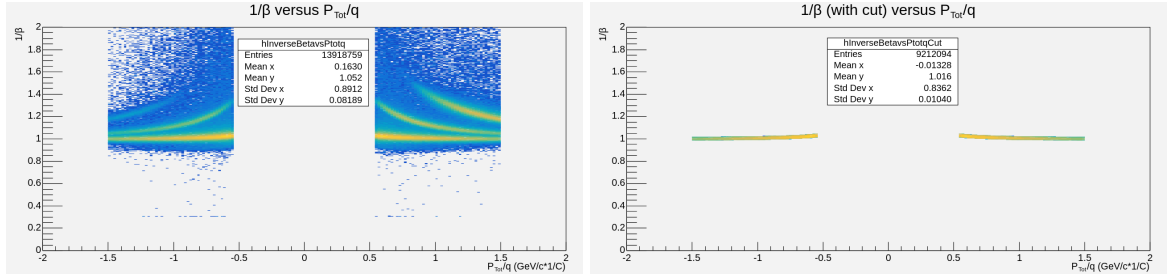


Figure A.16: The distribution of $1/\beta$ before and after PID

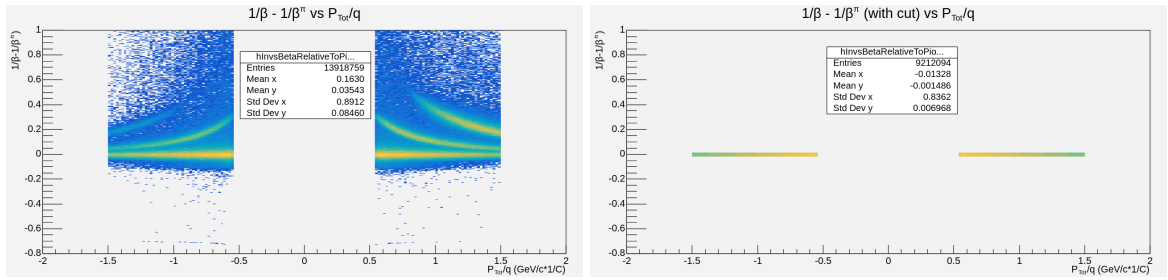


Figure A.17: The distribution of $1/\beta$ relative to $1/\beta_{\pi}^{expected}$ before and after the cut $1/\beta - 1/\beta_{\pi}^{expected} < 0.015$

A.4. Centrality

The centrality classes used for the analysis have been classified from the reference multiplicity in the following manner:

Centrality (%)	Reference Multiplicity
0 - 10	≥ 169
10 - 30	≥ 81
30 - 50	≥ 34
50 - 80	≥ 5

Table A.1: Distribution of centrality based on number of particle from reference multiplicity